Experimental Verification of PEEC Based Electric Field Simulations

Jonas Ekman

May 1999

Abstract

This paper describes how to model a electronic three-dimensional structure and its electromagnetic part with circuit variables instead of field variables as for commercial EM field solvers. The equivalent model is developed from an electric field integral equation and is applicable in the time and the frequency domain. The purpose with this master thesis is to evaluate the partial element equivalent circuit (PEEC) formulation with the circuit simulation program PSpice to characterize microwave circuits. For a constructed prototype the electric far field emitted should be computed using the PEEC model in PSpice and then verified with corresponding measurements. The PEEC theory was collected from various articles written by Ph. D. Albert E. Ruehli who has a large experience on the subject. A printed circuit board was manufactured and the corresponding PEEC model developed. Two different tests were performed to evaluate the PSpice simulations of the equivalent circuit. In the first test the input impedance of the test circuit was modeled with very good accuracy. In the second test the electrical far field emitted was calculated from the PSpice simulations. This was also done with good accuracy, but the results should be verified with a full wave EM solver since all field measurements are susceptible to noise interactions.

Contents

Preface

This paper is the final assignment for the Master of Science in Electrical Engineering at the University of Luleå. It was conducted at the Department of Industrial Electronics at the University and corresponds to 20 weeks of study. I would like to thank my examiner Prof. Jerker Delsing for giving me the opportunity to work with this interesting field, Åke Wisten for helping me with the PEEC theory and measurements conducted at the EMC Center, LTU. I would also like to thank Per Mäkikaltio for supplying equipment and components and Urban Lundgren for help with network analyzer measurements. Finally a thanks to Johan Carlson for help with Scientific WorkPlace.

Chapter 1

Introduction

1.1 Background

Electromagnetic interference is an important issue for all electronic equipment. The reason is that they must adhere to very strict standards for immunity and emission set by international EMC regulations. If excess radiation is detected, a portion of a product has to be redesigned and rebuilt resulting in increasing costs and product development time. The ability to predict the electromagnetic behavior of a system is then a valuable tool. This is possible in commercial thus expensive full wave solvers.

In this paper an alternative way of predicting the electromagnetic behavior of a circuit is presented. This is done with a partial element equivalent circuit (PEEC) model based on an electrical field integral equation full wave solution to Maxwell's equations. The model evolved from the partial inductance calculations for VLSI systems in 1972. Since then the model has been extended and corresponds now to a full wave method of moments solution. The PEEC model is formulated in circuit variables and compatible with circuit simulators such as PSpice where results can be obtained in the time and frequency domain. The extraction of the model parameters for the equivalent circuit and to use macromodeling techniques on complicated problems are the key issues in PEEC modeling.

In this paper the partial inductances of a test circuit are obtained from closed form equations. Since the partial capacitances are more difficult to calculate a three-dimensional capacitance extraction program called FastCap is used. Macromodeling techniques are used to develop the resultant PEEC model even though the test circuit is a simple printed circuit board.

1.2 Goal

The goal of this paper is to use the PEEC formulation with the circuit simulator program PSpice to model electronic systems. The accuracy of the developed PEEC model should be verified with appropriate tests including an electrical far field simulation.

1.3 Contents

This paper begins with the theoretical development of the PEEC model from the integral equation formulation. The interpretation of the theoretical model is followed by the evaluation of the partial elements and some important additions to the PEEC model. In chapter 6 the test circuit is presented and the corresponding equivalent circuit developed. Two different tests are performed and finally conclusions and propositions for further studies are drawn.

Chapter 2

Basic PEEC theory

The unknowns in a multiconductor system are the charges on the surfaces and the current densities within the conductors. An integral equation solution is appropriate for problems with large free-space regions since a differential equation formulation would require that all regions including the free space be described by nodes.

2.1 Development of PEEC model

The approximate integral equation solution pursued here is based on the proper electromagnetic interpretation of the various terms in the equation describing the sum of all the sources of electric fields at any point in space

$$\overline{E}(\overline{r},t) = \frac{\overline{J}(\overline{r},t)}{\sigma} + \frac{\partial \overline{A}(\overline{r},t)}{\partial t} + \nabla\Phi(\overline{r},t) \tag{2.1}$$

where $\overline{E}$ is the incident electric field, $\overline{J}$ is the current density in the conductor and $\overline{A}$ and Φ are the vector magnetic and scalar electric potentials respectively. The potentials are defined in a K conductor system by

$$\overline{A}(\overline{r},t) = \sum_{k=1}^{K} \frac{\mu}{4\pi} \int_{v_k} \frac{\overline{J}(\overline{r}',t')}{|\overline{r}-\overline{r}'|} dv' \tag{2.2}$$

and

$$\Phi(\overline{r},t) = \sum_{k=1}^{K} \frac{1}{4\pi\varepsilon} \int_{v_k} \frac{q(r',t')}{|\overline{r}-\overline{r}'|} dv' \tag{2.3}$$

where $\overline{r}$ is the vector to the field point and $t' = t$ - $|\overline{r}-\overline{r}'|$ / v denotes the retardation time in a medium with propagation speed v and q is the charge density. For simplicity the media surrounding the conductors are assumed to be homogeneous with permeability μ and permittivity ε. By inserting the definitions for the potentials 2.2 and 2.3 in 2.1 we obtain an expression involving the unknown current and charge densities

$$\frac{\overline{J}(\overline{r},t)}{\sigma} + \frac{\partial}{\partial t}\sum_{k=1}^{K} \frac{\mu}{4\pi} \int_{v_k} \frac{\overline{J}(\overline{r}',t')}{|\overline{r}-\overline{r}'|} dv' + \sum_{k=1}^{K} \frac{1}{4\pi\varepsilon} \nabla \left[\int_{v_k} \frac{q(\overline{r}',t')}{|\overline{r}-\overline{r}'|} dv' \right] = 0 \tag{2.4}$$

where σ is the conductivity at the specific point inside the conductor and the incident field is set to 0, which is used throughout the paper. In order to solve the system of equations in 2.4, the current and the charge densities are discretized into volume and surface cells, respectively. The volume cell give a 3-D representation of the current flow through a finite cross section, while the surface cells effect a 2-D representation of the charge over the surface of the corresponding volume cell. This discretization is achieved mathematically by defining the rectangular pulse functions

$$P_{\gamma nk} = \begin{array}{l} 1, \text{ inside the nkth volume cell} \\ 0, \text{ elsewere} \end{array} \tag{2.5}$$

for the current density where γ = x, y, z indicates the component of the current in the nth volume cell of the kth conductor, and

$$p_{mk} = \begin{array}{l} 1, \text{ on the mkth surface cell} \\ 0, \text{ elsewere} \end{array} \tag{2.6}$$

for the charge density on the mth surface cell of the kth conductor. The level of discretization is determined by the shape of the conductor, the shape of the surrounding conductors, and the frequency range of interest. In most applications it is acceptable to use 1-D or 2-D current distribution. But in more complicated situation like when skin effects are to be modeled a full 3-D distribution is required. Figure 2.1 shows the top view of a conductor and how it is segmented into volume cells with discretized two-dimensional current flow. Figure 2.2 shows the discretization of the charge density on the same conductor.

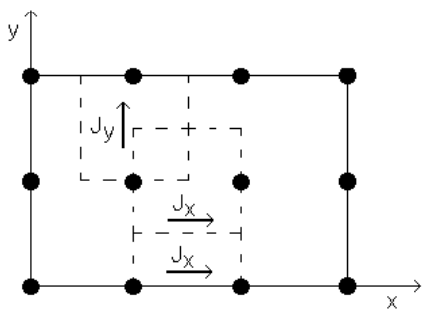

Figure 2.1: 2-D discretization of current desity

Given the definitions of the pulse functions in 2.5 and 2.6, the current and charge densities are approximated over each of the conductors by

$$J_{\gamma k}(\overline{r}, t') = \sum_{n=1}^{N_{\gamma k}} P_{\gamma nk} J_{\gamma nk}(t_n) \tag{2.7}$$

and

$$q_k(\overline{r}, t') = \sum_{m=1}^{M_k} p_{mk} q_{mk}(t_m) \tag{2.8}$$

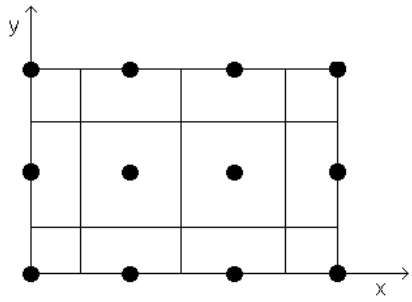

Figure 2.2: 2-D discretization of charge density

where t_n = t - $|\overline{r} - \overline{r}'_n|$ / v, t_m = t - $|\overline{r} - \overline{r}'_m|$ / v, $\overline{r}'_n$ is the position vector of the nth volume cell and $\overline{r}'_m$ is the position vector of the center of the equipotential surface associated with the mth surface cell. Additionally, $N_{\gamma k}$ denotes the number of the of volume cells for conductor k with γ directed current flow and M_k denotes the number of surface cells for conductor k. Substituting 2.7 into 2.4, we get for a point inside the mth cell of the lth conductor

$$\frac{J_{\gamma ml}(t)}{\sigma} + \frac{\partial}{\partial t}\sum_{k=1}^{K}\sum_{n=1}^{N_{\gamma k}}\frac{\mu}{4\pi}\left[\int_{v_k}\frac{P_{\gamma nk}J_{\gamma nk}(t_n)}{|\overline{r}-\overline{r}'|}dv'\right] + \sum_{k=1}^{K}\frac{\partial}{\partial t}\left[\frac{1}{4\pi\varepsilon}\int_{v_k}\frac{q(\overline{r}',t')}{|\overline{r}-\overline{r}'|}dv'\right] = 0 \quad (2.9)$$

This is followed by the testing of the resulting equation in the Galerkin approximation sense [20] utilizing an inner product over the volume of a cell defined as follows:

$$\frac{1}{a_m}\int_{v_m} f(\overline{r})dv = \frac{1}{a_m}\int_{a_m}\int_{l_m} f(\overline{r})dadl \quad (2.10)$$

where v_m is the volume of cell m, a_m is the cross section of the cell, l_m is its length, and $f(\overline{r})$ is the integrand. This process leads to a system of equations of the form

$$\frac{I_{\gamma ml}(t)l_m}{a_{\gamma ml}\sigma} + \sum_{k=1}^{K}\sum_{n=1}^{N_{\gamma k}}\frac{\mu}{4\pi}\frac{1}{a_{\gamma ml}}\frac{1}{a_{\gamma nk}}\int_{v_{ml}}\int_{v_{nk}}\frac{\frac{\partial}{\partial t}I_{\gamma nk}(t_n)}{|\overline{r}-\overline{r}'|}dv'dv_{ml} \quad (2.11)$$
$$+\sum_{k=1}^{K}\frac{1}{4\pi\varepsilon}\int_{v_{ml}}\frac{\partial}{\partial\gamma}\int_{S_k}\frac{q(\overline{r}',t')}{|\overline{r}-\overline{r}'|}ds'dv_{ml} = 0$$

where we make the identification that $J\gamma(t) = I\gamma(t)$ / a and convert the volume integration to a surface integration for the third term since the charge only resides on the surface of the volume.

Next, the approximation

$$\int_{v_l}\frac{\partial}{\partial\gamma}F(\gamma)dv_l \approx a_l\left[F(\gamma+\frac{l_m}{2}) - F(\gamma-\frac{l_m}{2})\right] \quad (2.12)$$

is used with 2.8 to reduce the last term in 2.11 to

$$\frac{I_{\gamma ml}(t)l_m}{a_{\gamma ml}\sigma} + \sum_{k=1}^{K}\sum_{n=1}^{N_{\gamma k}} \frac{\mu}{4\pi}\frac{1}{a_{\gamma ml}}\frac{1}{a_{\gamma nk}}\int_{v_{ml}}\int_{v_{nk}} \frac{\frac{\partial}{\partial t}I_{\gamma nk}(t_n)}{|\overline{r}-\overline{r}'|}dv'dv_{ml} \tag{2.13}$$
$$+\sum_{k=1}^{K}\sum_{m=1}^{M_k}\left[q_{mk}(t_m)\frac{1}{4\pi\varepsilon}\int_{S_{mk}}\frac{1}{|\overline{r}^+-\overline{r}'|}ds' - q_{mk}(t_m)\frac{1}{4\pi\varepsilon}\int_{S_{mk}}\frac{1}{|\overline{r}^--\overline{r}'|}ds'\right] = 0$$

This is the desired form of the discrete approximation of the electric field integral equation, from which the various types of the equivalent circuits can be inferred. Each term of 2.13 will now be discussed separately.

2.2 Resistive term

The first term in 2.13 is recognized to be the resistive voltage drop along the cell since the cell resistance is $\frac{l}{\sigma \cdot a}$. In the example given in this paper, we assume that the resistance is very small and that it can be ignored. The implementation of the resistive term will be discussed in chapter 5.1.

2.3 Inductance term

If the second term in 2.13 is rewritten to

$$\sum_{k=1}^{K}\sum_{n=1}^{N_{\gamma k}}\left[\frac{\mu}{4\pi}\frac{1}{a_{\gamma ml}}\frac{1}{a_{\gamma nk}}\int_{v_{ml}}\int_{v_{nk}}\frac{1}{|\overline{r}-\overline{r}'|}\,dv'\,dv_{ml}\right]\frac{\partial I_{\gamma nk}(t_n)}{\partial t} \tag{2.14}$$

the term in the brackets can be recognized to be in the form of partial inductances, $Lp_{ml,\gamma nk}$ and 2.14 can be rewritten as

$$\sum_{k=1}^{K}\sum_{n=1}^{N_{\gamma k}} Lp_{ml,\gamma nk}\frac{\partial I_{\gamma nk}(t_n)}{\partial t} \tag{2.15}$$

with the sums representing the coupling among them. Partial inductances will be covered in detail in chapter 3.

2.4 Capacitive term

To show that the last term in 2.13 correspond to capacitive coupling we make use of that the total charge on the mkth cell is given by $Q_{mk} = q_{mk} \cdot a_{mk}$ then the capacitive term in 2.13 can be rewritten as

$$\sum_{k=1}^{K}\sum_{m=1}^{M_k} Q_{mk}(t_{mk})\left[pp^+_{i(mk)} - pp^-_{i(mk)}\right] \tag{2.16}$$

where

$$pp_{ij} = \frac{1}{a_j} \int_{S_j} \frac{1}{4\pi\varepsilon} \frac{1}{|\overline{r}_i - \overline{r}'|} ds' \tag{2.17}$$

Then equation 2.17 can be interpreted as coefficients of potential which is covered in detail in chapter 4.

Chapter 3

Partial inductances

This section describes how to interpret and calculate the partial inductance part of the electrical field integral equation developed in chapter 2.

3.1 Definition of partial inductance

Inductance is traditionally thought of as a property of a closed loop. But the concept of partial inductances make it possible to ascribe portions of this loop inductance to segments of the loop. This must not be mistaken for the internal inductance of the conductor due to magnetic flux internal to the conductor. This is not the dominant inductance of the conductor since it decreases as the inverse square root of the frequency due to skin effect. It is dominated by an external inductance, the partial inductance of the segment, that is frequency independent. Partial inductances are named Lp_{ij} in order to distinguish them from loop inductances L_{ij}. The choice of the segments, or partitions, into which a circuit is divided is not unique. The lines dividing the conductor into parts, for which the partial inductances are to be calculated, are called inductive partitions see figure 3.1. Figure 3.1

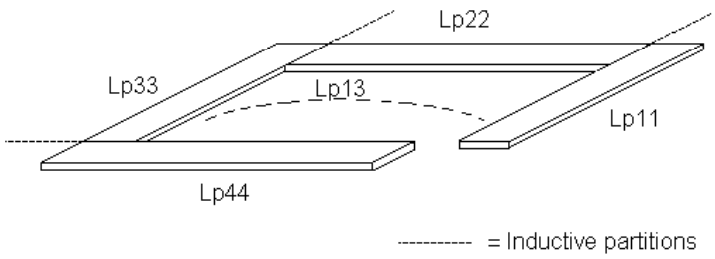

Figure 3.1: Conductor with inductive partitions

shows an important quality of the partial inductance concept, the ability to break a three dimensional problem into its constituent interactions. The partial inductance equivalent circuit of the loop in figure 3.1 is specified in terms of self partial inductances, Lp_{ii} of

the ith segment, and mutual partial inductances, Lp_{ij} between the ith and jth segments. If the loop is closed so that the same current flows through all segments the total loop inductance can be obtained with conventional circuit theory as

$$L = \sum_{i=1}^{4} \sum_{j=1}^{4} Lp_{ij} \tag{3.1}$$

The self partial inductance of a conductor, or segment of a conductor, is defined as the ratio of the magnetic flux generated by current I that passes between the conductor and infinity divided by the current I that produces it. And the mutual partial inductance between two conductors that are parallel and separated by a distance r_{ij} are defined as the ratio of the magnetic flux due to the current in the first conductor that passes between the second conductor and infinity to the current in the first conductor that produced it, this is shown in figure 3.2. From this definition we realize that there are no mutual inductances between perpendicular conductors. As for the geometry in figure 3.1 we conclude that $Lp_{23} = Lp_{32} = 0$, $Lp_{21} = Lp_{12} = 0$, $Lp_{34} = Lp_{43} = 0$ and $Lp_{14} = Lp_{41} = 0$. From the

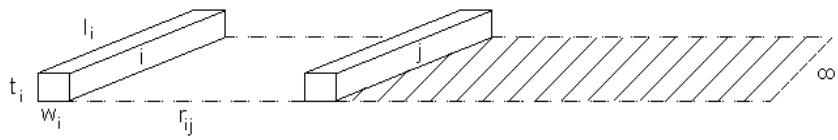

Figure 3.2: Figure for partial mutual inductance definition

definition, the mutual partial inductance can be written as [20]

$$Lp_{ij} = \frac{\int_{c_i} \overline{A}_{ij} \cdot d\bar{l}_i}{I_j} \tag{3.2}$$

where $\overrightarrow{A}_{ij}$ is the magnetic vector potential along segment l_i due to current I_j on segment l_j. When $i = j$ we define the self partial inductance of a conductor as

$$Lp_{ii} = \frac{\int_{c_i} \overline{A}_{ii} \cdot d\bar{l}_i}{I_i} \tag{3.3}$$

where $\overrightarrow{A}_{ii}$ is the magnetic vector potential along segment l_i due to current I_i on segment l_i. By using the magnetic vector potential given by

$$\overline{A}_{ij} = I_j \frac{\mu}{4\pi} \int_{b_i}^{c_i} \frac{d\bar{l}_j}{r_{ij}}$$

in 3.2 a expression for the partial inductance is obtained

$$Lp_{ij} = \frac{\mu}{4\pi} \int_{b_i}^{c_i} \int_{b_j}^{c_j} \frac{d\bar{l}_j \, d\bar{l}_i}{r_{ij}} \tag{3.4}$$

similar to $Lp_{ml,\gamma nk}$ in 2.15 which is the average mutual partial inductance over a cross section of a conductor.

With the current notations we can express the average partial inductance based on equation 3.4 as

$$Lp_{ij} = \frac{\mu}{4\pi}\frac{1}{a_i a_j}\int_{a_i}\int_{a_j}\int_{b_i}^{c_i}\int_{b_j}^{c_j}\frac{\left|d\bar{l}_i \cdot d\bar{l}_j\right|}{r_{ij}}da_i da_j \tag{3.5}$$

where b_i and b_j are start coordinates for the conductors i and j and c_i and c_j are the end coordinates.

3.2 Evaluation of partial inductances

3.2.1 Evaluation of self partial inductances

Self partial inductances are evaluated from equation 3.5, where integration i and j are both over the same conductor, or

$$Lp_{ii} = \frac{\mu}{4\pi}\frac{1}{a_i a_{i'}}\int_{a_i}\int_{a_{i'}}\int_{b_i}^{c_i}\int_{b_{i'}}^{c_{i'}}\frac{\left|d\bar{l}_i \cdot d\bar{l}_{i'}\right|}{r_{ii'}}da_i da_{i'} \tag{3.6}$$

The evaluation of equation 3.6 is complex, time consuming and susceptible to numerical errors. But approximate closed form solutions have been presented for rectangular conductors in [1] and [5]. These computations are performed with different equations depending on the aspect ratio of the conductor. The first and most general equation are named KS and is accurate for moderate conductor lengths. The second equation are for thin conductors and are named TS and the last equation named LS are for very long conductors. The formulas are invoked according to an decision algorithm presented in [5].

Algorithm 1 (decision for self partial inductance)
M = t / w ; U = l / w * Normalization's according to figure 3.2.
If (M > 1) then M=1 / M
If (U > 0.1) $\wedge$ (M < 0.0003) use TS
If (U > 80) $\wedge$ (M > 0.0003) use LS
If (U < 0.1) $\wedge$ (2E-5 < M < 0.0003) use KS
If (U < 80) $\wedge$ (M > 0.0003) use KS

For example the equation for very long conductors, LS, is given by

$$\frac{Lp_{ii}}{l} = \frac{\mu}{2\pi}\left[\ln\frac{2U}{1+M} + 0.5 + \frac{2}{9U(1+M)}\right] \tag{3.7}$$

and the other equations, KS and TS, are listed in appendix A.

3.2.2 Conductors of arbitrary cross section

For conductors other then the rectangular ones, a general formula for the self partial inductance is used. For a straight conductor k of length l with an arbitrary cross section, the conductor cross section is approximated by a set of N subconductors, called filaments, each having rectangular cross section. Then the self partial inductance is given by [1]

$$Lp_{ii} = \left[2 \sum_{i=1}^{N-1} \sum_{j=i+1}^{N} cof(Lp_{ij}) + \sum_{i=1}^{N} cof(Lp_{ii}) \right]^{-1} \det(Lp) \tag{3.8}$$

where cof indicates the cofactor of the element in the filament inductance matrix and det is the determinant. This formula is not used in this paper since all self partial inductances of interest are calculated using the KS equation according to decision algorithm 1.

3.2.3 Evaluation of mutual partial inductances

The evaluation of mutual partial inductances are all according to equation 3.5. To speed up the evaluation is important since it is invoked N^2 times, rather than N times like the self term evaluation. Here as for the evaluation of the self partial inductance Ruehli presents a decision algorithm and two closed form solutions [5] for the mutual partial inductances.

Algorithm 2 (decision for mutual partial inductance)
Mi = Ti / Wi; Mj = Tj / Wj
If (Mi > 0.002) $\wedge$ (Mj > 0.002) use TT
else use FF

Here TT stands for the thin tape - tape algorithm which is used for thin conductors, thickness to width ration > 0.002. The formulation of the TT equation is in Appendix B. The computations of the mutual partial inductances in this paper are done with this algorithm. For more "thick" conductors the FF algorithm is used, FF stands for filament - filament for mutual. Here as for the case of conductors of arbitrary cross sections, chapter 3.2.2, the conductors are divided in filaments. The mutual partial inductances are computed between all filaments, Lpf_{ij}, and are averaged to the mutual partial inductance as

$$Lp_{km} = \lim_{\substack{K \to \infty \\ M \to \infty}} \frac{1}{KM} \sum_{i=1}^{K} \sum_{j=1}^{M} Lpf_{ij} \tag{3.9}$$

For practical evaluation of equation 3.9 only a finite number of filaments are used [1] . The equation for the evaluation of the filaments mutual partial inductances is presented in appendix C.

3.2.3.1 Special cases for mutual partial inductances

Since the evaluation of the self partial inductances are easier there is much to gain if we can use these to evaluate the mutual partial inductances. In 1972 Ruehli presented a theorem for evaluation of mutual partial inductances for conductors on the same axis using this principle. This theorem is used in this paper to evaluate some mutual partial inductances and is simple to use. It requires two conductors k and m on the same axis of lengths l_k and l_m, with identical and arbitrary cross sections, $a_k = a_m$. Let the self partial inductance of a conductor i with same cross section and length $l_i = l_k + l_m$ be called Lp_{ii}. Then

$$Lp_{km} = \frac{1}{2}\left[Lp_{ii} - Lp_{kk} - Lp_{mm}\right] \tag{3.10}$$

if the two conductors are a continuation of each other , and

$$Lp_{km} = \frac{1}{2}\left[Lp_{ll} - Lp_{qq} - Lp_{oo} + Lp_{nn}\right] \tag{3.11}$$

if the conductors are separated by a distance l_n. Lp_{ll} is the inductance of a conductor length $l_m + l_k + l_n$, and Lp_{oo}, Lp_{qq} refer to the inductance of conductors length $l_m + l_n$ and $l_k + l_n$ respectively. A proof is presented in [1] for the first case. Also a theorem for parallel conductors with one parallel side touching is presented in the same paper. This is not used in this paper and will not be repeated here.

3.3 Equivalent circuit with partial inductances

To be able to analyze the desired structure we must transform it into an equivalent circuit. After the partitioning of the system into suitable inductive partitions and the evaluation of partial inductances nodes are introduced. Every inductance partition starts and ends with a node and the nodes interconnects with the corresponding self partial inductance. Figure 3.3 displays the circuit in figure 3.1 with numbered nodes.

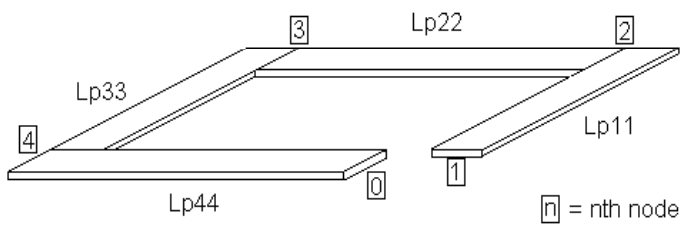

Figure 3.3: Conductor with nodes and self partial inductance partitions

The circuit in figure 3.3 can be implemented in a PSpice text file or in PSpice Schematics as in figure 3.4.

It is possible for some cases to use only the partial inductances for a simplified PEEC model, see chapter 5, but for the tests performed later the capacitive couplings are also used.

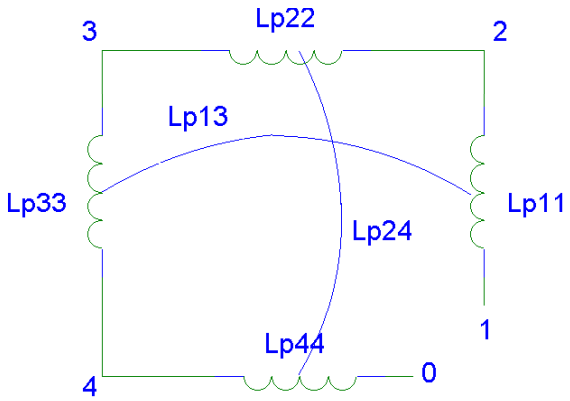

Figure 3.4: Equivalent circuit with partial inductances and numbered nodes

Chapter 4

Coefficients of potential

4.1 Capacitive representation

Capacitive coupling can be implemented in different ways in the PEEC model. Depending on the application one way can offer several advantages over the others and for other cases produce wrong results. This chapter focus on different capacitive coupling representations and the evaluation of these.

4.1.1 Coefficients of potential

In chapter 2.4 we concluded that equation 2.17 was in the form of coefficients of potential. The definition of the coefficients of potential in matrix form is

$$\mathbb{V} = \mathbb{P}\mathbb{Q} \tag{4.1}$$

where $\mathbb{V}$ is the vector of segment potentials, $\mathbb{Q}$ represents the total segment charge and $\mathbb{P}$ the matrix of coefficients of potentials for the partitioned system. From equation 4.1 we see that equation 2.16 represents the voltage differences across the elements since $pp^{+}_{i(mk)}$ and $pp^{-}_{i(mk)}$ is the partial coefficient of potential associated with the positive and negative end of the mkth cell respectively. A closed form answer [2] for the coefficients of potential for parallel cells can be found in appendix D.

4.1.2 Short circuit capacitances

The inverse of the partial coefficient of potential matrix is called the short circuit capacitance matrix, $\mathbb{C}_s$. The transformation from the coefficients of potential matrix to the short circuit capacitance matrix can only be done if no time retardation (no delay time between capacitive partitions) is accounted for. This issue will be discussed more in detail in chapter 5.2. If $\mathbb{Q}$ is the vector of total charges on the segments and $\mathbb{V}$ the segment potentials then

$$\mathbb{Q} = \mathbb{C}_s\mathbb{V} \tag{4.2}$$

thus

$$\mathbb{C}_s = \mathbb{P}^{-1} \tag{4.3}$$

The positive diagonal terms of $\mathbb{C}_s$ are called coefficients of capacitance while the negative off diagonal terms are called coefficients of electrostatic induction.

4.1.3 Partial capacitances

In conventional network analysis programs the capacitance between different conductors, or segments of conductors, of different potentials are expressed as terminal capacitances. To illustrate this consider the four conductor problem shown in figure 4.1. The equivalent circuit in figure 4.2 is in terms of the two terminal capacitances defined as

$$C_{ij} = \frac{Q_{ij}}{V_i - V_j} \tag{4.4}$$

where Q_{ij} is the charge associated with this capacitance, V_i is the potential of the ith conductor, and $C_{ij} = C_{ji}$. From this definition a $N \times N$ capacitance matrix, $\mathbb{C}$, for a N conductor system is constructed. Here the diagonal terms, C_{ii}, are called self capacitances and the off diagonal terms, C_{ij}, mutual capacitances. These are the capacitances that are called partial capacitances, Cp_{ij}, when dealing with segmented conductors.

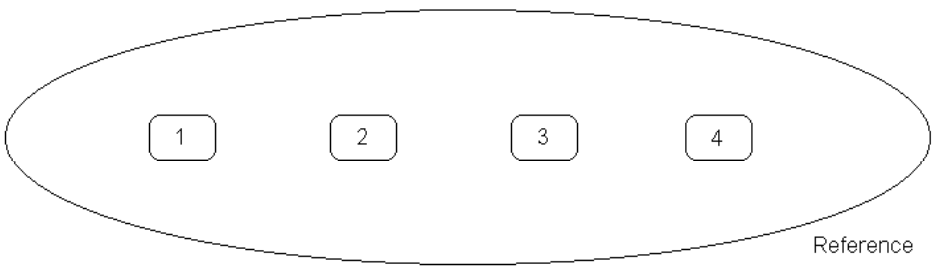

Figure 4.1: Four conductor geometry

The relationship between the elements in the short circuit capacitance matrix, $\mathbb{C}_S$, and the capacitance matrix, $\mathbb{C}$, is developed from the definitions. And the capacitance matrix, $\mathbb{C}$, can be expressed in terms of the short circuit capacitances as

$$\mathbb{C} = \begin{bmatrix} \sum_{j=1}^{4} C_{S1j} & -C_{S12} & -C_{S13} & -C_{S14} \\ -C_{S21} & \sum_{j=1}^{4} C_{S2j} & -C_{S23} & -C_{S24} \\ -C_{S31} & -C_{S32} & \sum_{j=1}^{4} C_{S3j} & -C_{S34} \\ -C_{S41} & -C_{S42} & -C_{S43} & \sum_{j=1}^{4} C_{S4j} \end{bmatrix}$$

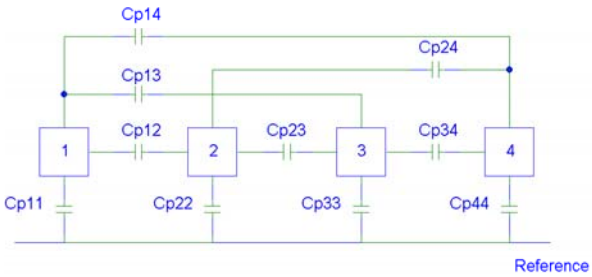

Figure 4.2: Equivalent circuit for four conductors

When dealing with very complex problems the capacitance matrices are very big, then a computer implementation of the conversation is desirable. This can be done with the following algorithms presented in [4]

$$C_{ii} = \sum_{j=1}^{N} C_{Sij} \qquad i = 1, 2, ..., N \tag{4.5}$$

$$C_{Sii} = \sum_{j=1}^{N} C_{ij} \qquad i = 1, 2, ..., N \tag{4.6}$$

$$C_{Sij} = -C_{ij} \qquad for \qquad i \neq j \tag{4.7}$$

4.1.4 Node-pair capacitances

An additional way to represent capacitive coupling is by the use of node-pair capacitances [4]. This is a way to exclude the capacitive coupling to the reference conductor. This can be useful to facilitate analytical analysis of circuits. The simplification achieved is shown for the four conductor problem in figure 4.1 by comparing the equivalent circuit with terminal capacitances, figure 4.2, with the equivalent circuit with node-pair capacitances in figure 4.3.

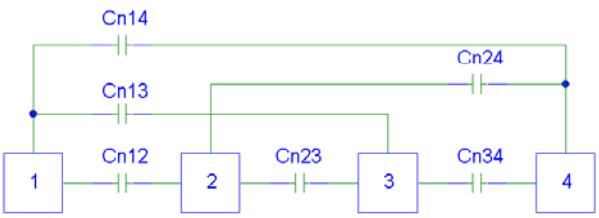

Figure 4.3: Node-pair capacitance representation

The transformation from the $\mathbb{C}$-matrix to the $\mathbb{C}_n$-matrix for a k conductor system is done with the following algorithms presented in [4]

$$C_{nij} = C_{ij} + \frac{C_{ii}C_{jj}}{C_\Sigma} \tag{4.8}$$

where

$$C_\Sigma = \sum_{j=1}^{k} C_{jj} \tag{4.9}$$

The diagonal coefficients of the node-pair capacitance matrix are removed since they correspond to the eliminated reference conductor at infinity. Node-pair capacitances have been used in chapter 7.1 for evaluation of the principle. The conclusion is that they should not be used in computer aided analysis of circuits since its a approximate capacitance representation.

4.2 Evaluation of partial capacitances

4.2.1 Capacitive partitioning

An important observation from equation 2.12, the approximation of the integral in the γ coordinate, is that the capacitive cells are shifted from the inductive cells by half the size of a cell [3]. To illustrate this figure 3.1 is used with the capacitive partitions added.

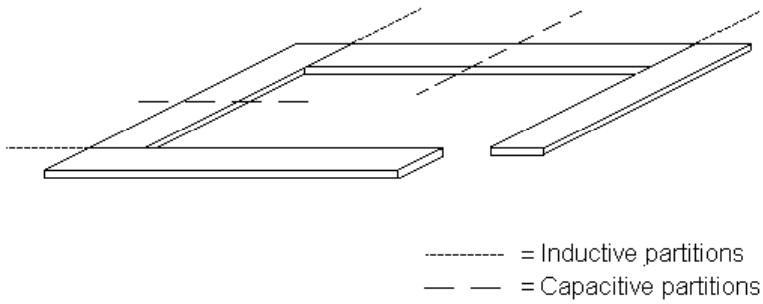

Figure 4.4: Conductor with inductive and capacitive partitions

As can be seen in figure 4.4, the geometry of the capacitive partitions are three L-shaped conductors of different proportions. To evaluate the coefficients of potential for this simple geometry and then obtain the partial capacitances is quite complex. It is desirable to use a three-dimensional capacitance extraction program for the evaluation of the partial capacitances used in the computer simulations. A program well suited for this is a freeware program developed at MIT in 1992 called FastCap [25].

4.2.2 FastCap - A 3D capacitance extraction program

FastCap is a three-dimensional capacitance extraction program that computes self, C_{ii}, and mutual, C_{ij}, capacitances between ideal conductors of arbitrary shapes and sizes. The conductors can be embedded in dielectric regions of any shapes and of any number of constant permittivity. The program uses a boundary-element technique to solve the integral equation based on equation 2.17. To calculate the capacitance matrix for a partitioned conductor a input file containing the geometry must be constructed, executed in FastCap and then from the short-circuit capacitance matrix the terminal capacitances are calculated. These steps will now be explained in detail.

4.2.2.1 Preparing input files for FastCap

The geometry for which the capacitance matrix are to be calculated can be modeled with the CAD program MSC/PATRAN [24], or by a generic file format designed for FastCap. Since MSC/PATRAN is not in use at LTU the generic file interface must be used to model the conductors. This is done by building conductors from quadrilateral panels that are defined by its corner coordinates. This is not the best way to model conductors since FastCap requires additional partitioning of the already partitioned conductors to account for the edge effects. This is illustrated in figure 4.5 and 4.6. This results in a

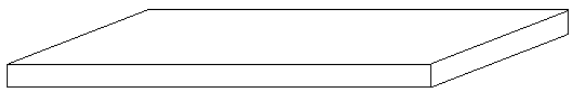

Figure 4.5: Original partial conductor

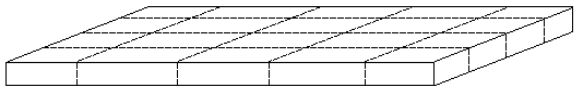

Figure 4.6: Desired discretization of the partial conductor

time consuming modeling process and is almost impossible for larger systems of partial conductors. But still FastCap is a good tool to extract partial capacitances. This is illustrated by comparing the partial coefficients of potential published in [11] with the results from a FastCap calculation. The problem in [11] consists of a single conducting zero thickness metal strip 2 cm wide and 10 cm long shown in figure 4.7. The conductor is divided into three numbered capacitive partitions as shown. Since FastCap does not accept zero thickness the thickness is set to 0.01cm. The input file to FastCap consists

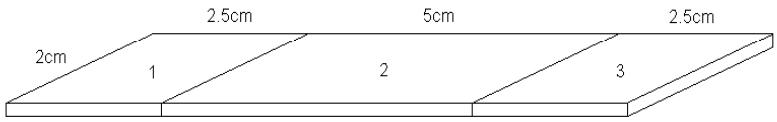

Figure 4.7: Metal strip

of a headline plus 14 lines specifying the panels that produces the conductor, each line starts with a Q plus the name of the capacitive partition.

0	Input file to	FastCap for metal	strip in fig. 4.7	
Q1	0 0 0	0.02 0 0	0.02 0.0001 0	0 0.0001 0
Q1	0 0 0	0.02 0 0	0.02 0 0.025	0 0 0.025
Q1	0 0.0001 0	0.02 0.0001 0	0.02 0.0001 0.025	0 0.0001 0.025
Q1	0 0 0	0 0 0	0 0.0001 0.025	0 0.0001 0
Q1	0.02 0 0	0.02 0 0.025	0.02 0.0001 0.025	0.02 0.0001 0
Q2	0 0 0.025	0.02 0 0.025	0.02 0 0.075	0 0 0.075
Q2	0 0.0001 0.025	0.02 0.0001 0.025	0.02 0.0001 0.075	0 0.0001 0.075
Q2	0 0 0.025	0 0 0.075	0 0.0001 0	0 0.0001 0.025
Q2	0.02 0 0.025	0.02 0 0.075	0.02 0.0001 0.075	0.02 0.0001 0.025
Q3	0 0 0.075	0.02 0 0.075	0.02 0 0.1	0 0 0.1
Q3	0 0 0.075	0.02 0 0.1	0.02 0.0001 0.1	0 0.0001 0.1
Q3	0 0.0001 0.075	0.02 0.0001 0.075	0.02 0.0001 0.1	0 0.0001 0.1
Q3	0 0 0.075	0 0 0.1	0 0.0001 0.1	0 0.0001 0.075
Q3	0.02 0 0.075	0.02 0 0.1	0.02 0.0001 0.1	0.02 0.0001 0.075

From this file FastCap produces a short circuit capacitance matrix

$$\mathbb{C}_S = \begin{bmatrix} 0.89 & -0.27 & -0.03 \\ -0.27 & 1.4 & -0.3 \\ -0.03 & -0.3 & 0.85 \end{bmatrix} \text{pF} \tag{4.10}$$

and from the matrix inversion of $\mathbb{C}s$ the coefficients of potential are obtained when no time retardation is accounted for. For this case the time retardation can be ignored up to approximately 300 MHz, see chapter 5.2.

$$\mathbb{C}_S^{-1} = \mathbb{P} = \begin{bmatrix} 1.2 & 0.26 & 0.13 \\ 0.26 & 0.83 & 0.31 \\ 0.13 & 0.31 & 1.3 \end{bmatrix} \text{pF}^{-1} \tag{4.11}$$

This matrix can be compared with the one published in [11]

$$\mathbb{P} = \begin{bmatrix} 1.2 & 0.30 & 0.12 \\ 0.30 & 0.8 & 0.30 \\ 0.12 & 0.30 & 1.2 \end{bmatrix} \text{pF}^{-1} \tag{4.12}$$

The conclusion is that FastCap produces good results compared to other approximate solutions as the one in [11]. For a perfect match for the coefficients of potential in matrix 4.12, the closed form solution for the coefficients of potential presented in Appendix D should be used.

4.2.2.2 Running FastCap

FastCap is executed with the input file and a short circuit capacitance matrix is produced. With certain options FastCap produces geometry, charge density and total charge pictures. With the ability to combine multiple files in a macro file, called list file, conductors can be placed in dielectric regions or between ground planes. With the possibility to set the accuracy in the computational algorithms the calculation time for big problems can be reduced.

4.2.2.3 FastCap results

After correct execution FastCap produces the systems short circuit capacitance matrix. The conversion to the terminal capacitances suitable for computer simulation is then done as explained in chapter 4.1.3.

4.3 Equivalent circuit with partial capacitances

After calculating the partial capacitances they are combined into a equivalent circuit as for the case with the partial inductances in chapter 3.3. In figure 4.8 the circuit from figure 3.1 are completed with the nodes and capacitive partitions.

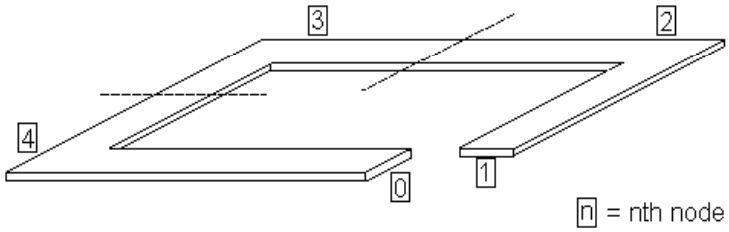

Figure 4.8: Conductor with capacitive partitions and numbered nodes

For the conductor in figure 4.8 a 3×3 capacitance matrix is calculated and then transformed into a equivalent circuit containing center nodes 2,3 and 4 as shown in figure 4.9. But the partial capacitances must be incorporated with the partial inductances in figure 4.2 or with the cell resistivity to form a valid equivalent circuit. The result with the partial inductances is the circuit in figure 4.10. This circuit can with advantage be written to a text file and then compiled with PSpice. The circuit in figure 4.10 is based on the simplest

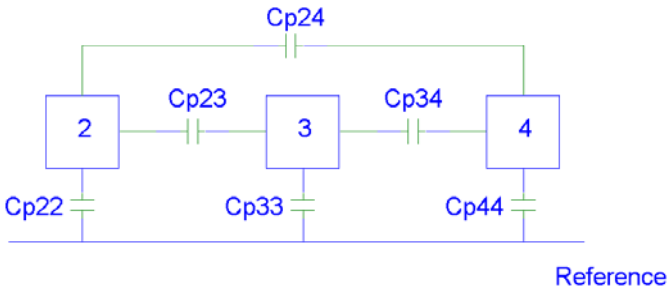

Figure 4.9: Partial capacitance equivalent circuit for the conductors in figure 4.8.

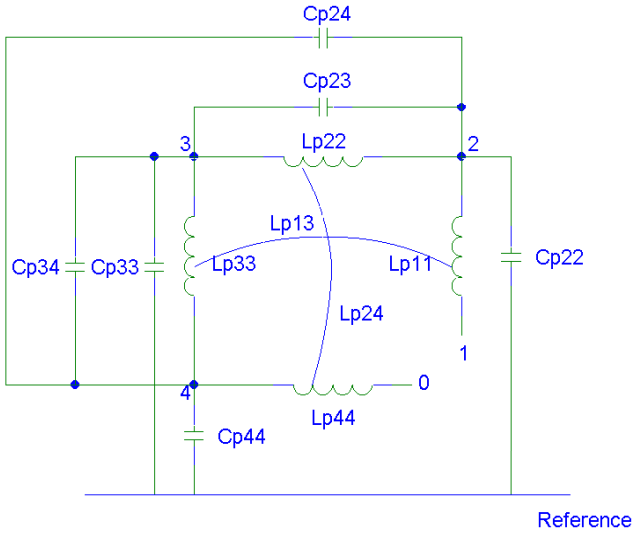

Figure 4.10: PEEC model of the circuit in figure 4.8

capacitive partitioning of the original circuit. Two more capacitive partitions could have been done, between node 4 and 0 and between node 1 and 2 in figure 4.8, resulting in a 5×5 capacitance matrix for the equivalent circuit. This would have been a more accurate model for the original circuit, but good agreement can be obtained with few partitions as will be seen later.

Chapter 5

Extended PEEC models

For a complete PEEC model the cell resistivity, time retardation and incident electric fields must be included in the equivalent circuit. It is not always necessary to incorporate all part of the full PEEC formulation. Macromodels obtained by reducing the complete PEEC formulation are used quite frequently. The full model is noted (R,Lp,P,τ,Vp)PEEC where the terms mean that the quantities are included in the PEEC part of the model. The notation which indicates the presence of at least one element of a particular type is R for cell resistance, Lp for partial inductances, P for the coefficients of potential, C for partial capacitances, τ for time retardation and Vp for potential incident field sources. Table 5.1 [15] gives most of the situations for reduced PEEC models.

Description	PEEC model
Full model	(R,Lp,P,τ)
All delays small	Ignore all τ (R,Lp,P)or(R,Lp,C)
Resistences small	(Lp,P,τ) or (Lp,C)
High currents. Chip power	(R,Lp) or (Lp)
Low currents. Chip. Signals	(R,P) or (R,C)

Table 5.1: PEEC model reduction

This chapter deal with all the additions to the (Lp,C)PEEC model that can be necessary to incorporate in the equivalent circuit.

5.1 Cell resistivity

It was concluded in chapter 2.2 that the first term of equation 2.13 describes the resistive voltage drop along the cell. This is simply the DC resistance in the direction of the current, and can easily be calculated from the conductivity of the conductor material. As noted in table 5.1 the cell resistance can be excluded from the PEEC model if it is small. The implementation of the cell resistance is best shown in a figure for a two-cell PEEC model example. A two-cell is a conductor that is divided in two identical inductive cells

with three nodes as in figure 5.1. The cell resistances are calculated for the two inductive partitions and thus equal.

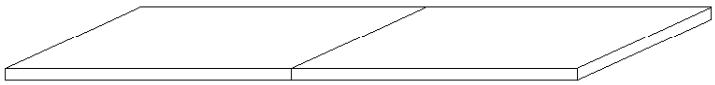

Figure 5.1: Conductor divided in two inductive cells

The (Lp,C)PEEC model for the two-cell conductor in figure 5.1 is shown in figure 5.2 and a (Lp,C,R)PEEC model in figure 5.3.

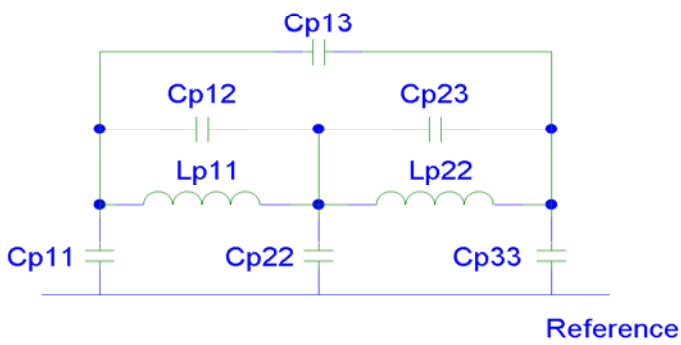

Figure 5.2: (Lp,C) PEEC model for two-cell conductor

In figure 5.3 the cell resistance is denoted Rsi for self resistance. The conclusion is that cell resistances are easy calculated and implemented in PEEC models but not always necessary, table 5.1.

5.2 Time retardation

The importance of time retardation becomes significant if the physical size of the structure under consideration becomes large or the frequency spectrum of the transients gets high. For cells in the structure that are far apart, the non retarded mutual partial inductances and mutual partial capacitances may couple with the wrong phase. A rule of thumb is that a tolerable phase error occurs if the cells in the problem with the largest physical distance fulfill the condition that

$$\tau_{ij}\, f_{max} << 1 \tag{5.1}$$

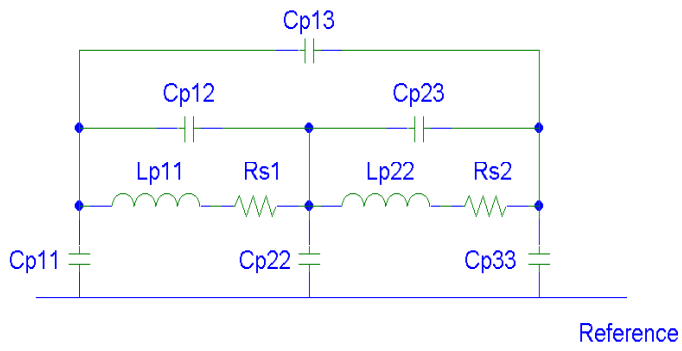

Figure 5.3: (Lp,C,R)PEEC model for two-cell conductor

where

$$\tau_{ij} = r_{ij}/c \tag{5.2}$$

is the delay time for the two cells involved, r_{ij} is the distance between conductor i and j, c is the speed of light and f_{max} is the maximum frequency in the spectrum of the transients. To include far coupling coefficients without the phase factor is worse than to leave the coupling factor out completely [13]. The way to include time retardation in the PEEC model will be presented in the following two sections resulting in a rPEEC model. This theory is valid only for a circuit solver in which the time delays defined by equation 5.2 can be incorporated.

5.2.1 Capacitive representation

From the definition of coefficients of potential, equation 4.1, the potential on conductor i can be expressed as

$$\Phi_i(t) = \sum_{j=1}^{n} p_{ij} Q_j(t'_{ij}) \tag{5.3}$$

where

$$t'_{ij} = t - \tau_{ij} \tag{5.4}$$

If $t'_{ij} = t$ (infinite speed of light) is assumed, equation 4.1 can be inverted into equation 4.3 to form the expression for the short circuit capacitance matrix. With retardation, $t'_{ij} \neq t$, equation 4.1 cannot be inverted and the capacitive coupling must be expressed in terms of the coefficients of potential. Such a circuit formulation is presented in [10]. It replaces the self partial capacitances of an arbitrary circuit by pseudo-capacitances, $c'_i = p_{ii}^{-1}$, and the mutual partial capacitances with controlled current sources, $I_{Ci}(t)$, as for the two-cell (C)PEEC example in figure 5.4. The controlled sources are derived from the definition

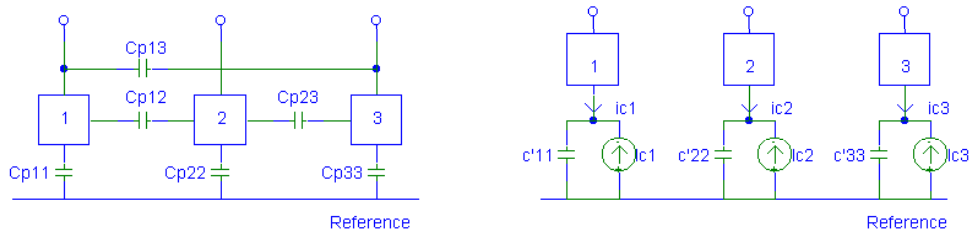

Figure 5.4: Transformation from terminal capacitances to pseudo capacitances with controlled current sources.

of the coefficients of potential and the current charge relationship $i = \frac{dQ}{dt}$. In general, by defining K capacitive cells in the problem the potential Φ_i on conductor i is given by

$$i_{ci}(t) = \frac{\Phi_i}{p_{ii}} - \sum_{j=1}^{K} \frac{p_{ij}}{p_{ii}} i_{cj}(t'_{ij}) \tag{5.5}$$

where $i_{ci}(t)$ is the total current for conductor i. Then the retarded current sources referenced in figure 5.4 are given by the following equations

$$I_{c1} = \frac{p_{12}}{p_{11}} i_{c2}(t'_{12}) + \frac{p_{13}}{p_{11}} i_{c3}(t'_{13}) \tag{5.6}$$

$$I_{c2} = \frac{p_{21}}{p_{22}} i_{c1}(t'_{21}) + \frac{p_{23}}{p_{22}} i_{c3}(t'_{23}) \tag{5.7}$$

$$I_{c3} = \frac{p_{31}}{p_{33}} i_{c1}(t'_{31}) + \frac{p_{32}}{p_{33}} i_{c2}(t'_{32}) \tag{5.8}$$

Time retardation is ignored in the tests performed later on since the condition in equation 5.1 applies to the test circuit for frequencies approximately under 800 MHz, see chapter 6.2.3.

5.2.2 Inductive representation

The inductive coupling represented by the mutual partial inductances in the PEEC model are handled in a very similar way. Here the coupling is represented by a voltage source, $V_L i(t)$, in series with the corresponding self partial inductance. The voltage source is given by

$$V_L i(t) = \sum_{j \neq i} \frac{Lp_{ij}}{Lp_{jj}} v'_j(t'_{ij}) \tag{5.9}$$

where $v'j$ is the voltage over the self partial inductance Lp_{jj} [8]. This transformation is illustrated in figure 5.5 for a (L)PEEC three-cell example.

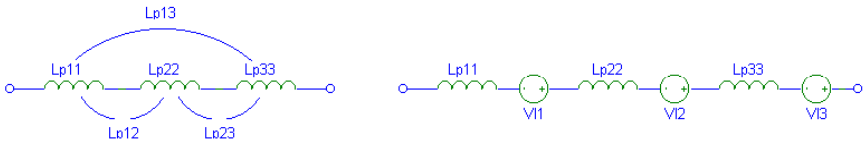

Figure 5.5: Transformation from no retarded model to retarded for inductive coupling

5.3 Incident fields

In the development of the PEEC model in chapter 2 the term describing the incident electric field, $\overline{E}$, in equation 2.1 was excluded. This is correct for all the tests done in this paper but is important for certain problems. The incident field part of the PEEC theory is solved with a voltage source formulation. This is best illustrated in a simple, 1D z-directed current distribution, example for the two-cell shown in figure 5.6. The equivalent

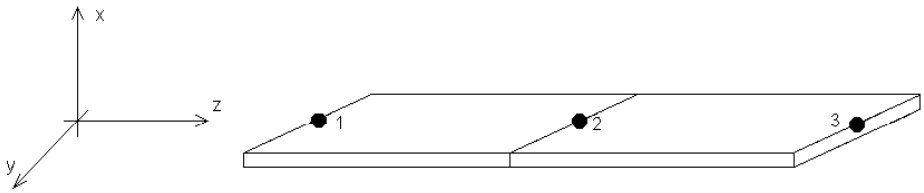

Figure 5.6: Two-cell for incident field example

(Lp,P)PEEC model with additions for the incident field representation is presented in figure 5.7. Here the additional Vpi sources are simply the induced voltage in the inductive

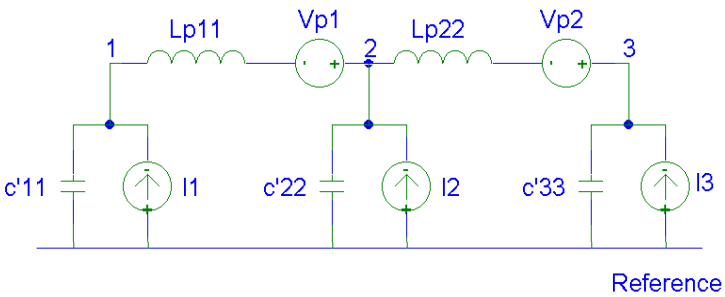

Figure 5.7: (Lp,P,Vp)PEEC model for circuit in figure 6.6

partitions. A general formulation for the induced voltage in the ith cell is

$$Vp_i(t_i') = \frac{1}{a_i} \int_{a_i} \int_{l_i} E_Z(\overline{r}, t_i') dadl \tag{5.10}$$

where a_i is the cross-section of the cell (x-y direction), l_i is the length (z-direction) and t_i' is the time of incidence at cell i and is given by

$$t_i' = t - \frac{|\overline{r} - \overline{r}'|}{c} \tag{5.11}$$

and the distance $|\overline{r} - \overline{r}'|$ is between the electric field source and the ith cell. For the example Vp2 is delayed with respect to Vp1 by $\frac{R_{12}}{c}$, where R_{12} is the center to center distance for the two cells. A complete example for this source formulation of incident fields in PEEC models are given in [10].

5.4 Dielectric regions

In [9] a theory to include finite dielectric regions in the PEEC model was developed. This do results in a more complicated PEEC model since the dielectrics are represented as internal nodes. But the extension makes the model analogous to a full-wave solution like commercial method of moments solvers. Since no dielectric regions are considered in the PEEC models developed later, this theory will not be reviewed here.

5.5 Model instability

It is important to know that the EFIE (Electrical Field Integral Equation) based PEEC formulation suffers from late time instability. In the time domain, the model instability will be observed as an unstable solution that will totally mask the real solution starting at some (late) point in time. An important finding was that models that are unstable in the time domain also show false resonances in the frequency domain [19]. The confusing aspect of the stability issue is that there may be two contributing factors that may cause instabilities. Instabilities may be due to either the numerical technique used for the time integration, or by the discrete representation for the numerical solution of the problem. These two sources of instability can be present at the same time in any particular discretized implementation. Different techniques to minimize these problems are presented in [11], [14], [17] and [18]. One is called the +PEEC model [18] where a new way of calculating the partial inductances and coefficient of potential terms is derived in order to stabilize the time domain solution and increase the accuracy for higher frequencies.

Chapter 6

The test circuit

6.1 Original circuit

6.1.1 Introduction

As was mentioned in the abstracts, one of the goals for this master thesis was to be able to implement a PEEC model for an arbitrary circuit. The circuit that was chosen is a simple voltage divider, with one or two additional capacitances, located on a dielectric substrate, figure 6.1. This circuit is presented in [3] and is well suited for our purposes since

1. A complete PEEC model exists in [3].
2. The circuit is suited for radiated field calculations, see chapter 8.
3. Macromodeling techniques can be applied, see chapter 5.

6.1.2 Reproducing model parameters

Since very few examples of complete PEEC models with corresponding partial elements have been published it was necessary to reproduce the results in [3] to test the theory described in chapter 3-5.

6.1.2.1 Partial inductances

The original circuit with corresponding inductive partitions and node numbers from [3] can be seen in figure 6.2 together with the (L)PEEC model. The height, 61mm, was the only distance that was given for the geometry unless for the conductors cross section, 1.2mm$\times$50μm. But the conductors were measured in a figure in [3] resulting in the approximate lengths in figure 6.2.

The decision algorithm for self partial inductances in chapter 3.2.1 together with the conductor lengths and cross sections suggested the use of the KS equation for the calculations. Table 6.1 shows the self partial inductances tabulated in [3] and the ones calculated with the KS equation.

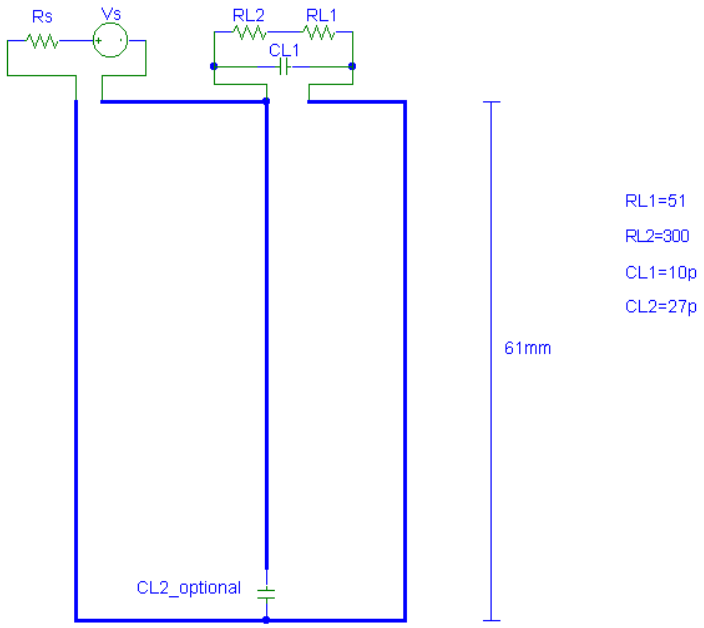

Figure 6.1: Original circuit

Inductive partition	Conductor length (mm)	Self ind. from [3] (nH)	Self ind. with KS equation. (nH)
Lp11	57	57.2	57.2
Lp22	13.9	10.2	10.1
Lp33	61	62.1	62.1
Lp44	15.4	11.6	11.5
Lp55	24.8	21	20.8
Lp66	58.5	59	59
Lp77	23.8	20	19.8

Table 6.1: Self partial inductances for figure 6.2

This good match for the self partial inductances are not surprising, they are calculated with the KS equation in [3].

The decision algorithm for mutual partial inductances in chapter 3.2.2 suggested the use of the TT equation for these calculations. Table 6.2 shows the mutual partial inductances tabulated in [3] and the ones calculated with the TT equation.

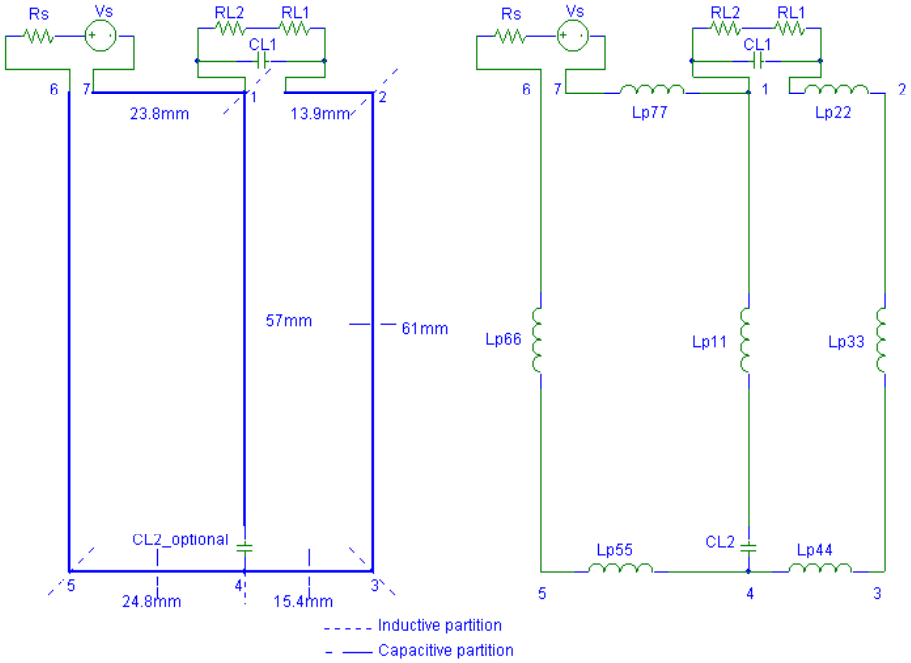

Figure 6.2: Original circuit and corresponding (L)PEEC model

Mutual ind. pair	Mutual ind. from [3]. (nH)	Mutual ind. calculated with TT equation. (nH)
Lp13	14.7	14.7
Lp16	10.6	10.6
Lp27	2	2.05
Lp36	7.7	8.22
Lp45	2.4	2.64
Lp57	1	0.97

Table 6.2: Mutual partial inductances for figure 6.2

As for the self inductances these values are well matched except for Lp36, this is probably because of inaccuracy when measuring the distance between inductive partition three and six in [3].

6.1.2.2 Partial capacitances

To evaluate the partial capacitances FastCap were used with the capacitive partitions numbered according to figure 6.3. The geometry was constructed in FastCap generic file format by describing 182 panels with 2184 corner coordinates and the capacitances were calculated without the presence of the dielectric substrate, see chapter 4.2.2.1. The resultant short circuit capacitance matrix calculated by FastCap is

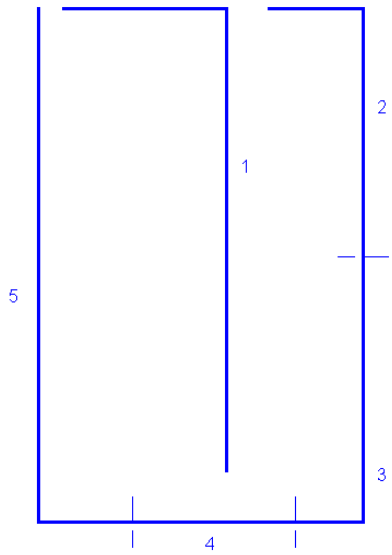

Figure 6.3: Numbered capacitive partitions for FastCap calculations

$$\mathbb{C}_S = \begin{bmatrix} 915 & -147 & -85 & -53 & -162 \\ -147 & 542 & -42 & -8 & -40 \\ -85 & -42 & 470 & -46 & -38 \\ -53 & -8 & -46 & 292 & -53 \\ -162 & -40 & -38 & -53 & 821 \end{bmatrix} \text{fF} \tag{6.1}$$

And the corresponding capacitance matrix is

$$\mathbb{C} = \begin{bmatrix} 468 & 147 & 85 & 53 & 162 \\ 147 & 305 & 42 & 8 & 40 \\ 85 & 42 & 259 & 46 & 38 \\ 53 & 8 & 46 & 132 & 53 \\ 162 & 40 & 38 & 53 & 528 \end{bmatrix} \text{fF} \tag{6.2}$$

To be able to compare these capacitances with the ones in [3], the node-pair capacitances from the capacitance matrix 6.2 must be calculated. This results in a node-pair capacitance matrix

$$\mathbb{C}_n = \begin{bmatrix} 0 & 231 & 157 & 90 & 308 \\ 231 & 0 & 89 & 32 & 135 \\ 157 & 89 & 0 & 66 & 119 \\ 90 & 32 & 66 & 0 & 94 \\ 308 & 135 & 119 & 94 & 0 \end{bmatrix} \text{fF} \tag{6.3}$$

These node-pair capacitances are tabulated with the ones from [3] in table 6.3.

Capacitance pair	Node-pair capacitances from [3]. (fF)	Node-pair capacitances from equation 6.3. (fF)
Cp12	610	231
Cp13	525	157
Cp14	225	90
Cp15	725	308
Cp23	285	89
Cp24	not tabulated	32
Cp25	275	135
Cp34	125	66
Cp35	275	119
Cp45	225	94

Table 6.3: Node-pair capacitances for figure 6.3

A mismatch was expected since the capacitances in [3] are calculated with the impact of the dielectric substrate, but that could not solely affect the capacitances this much. After contacting Mr. Ruehli on this question he explained that the capacitances in [3] may not be too accurate since they were at the beginning of capacitance calculations with dielectric blocks. This letter is included in Appendix E. The conclusion is that we can use FastCap for approximate capacitance calculations since it do produce accurate results for dielectric free geometry's as in chapter 4.2.2.1. But better results can be obtained by using MSC/PATRAN modeled conductors and dielectric regions.

6.1.3 Reproducing PEEC model test

In [3] the voltage time domain response over RL_2 in figure 6.1 was examined for a unit step input signal at Vs. This test was performed with and without CL_2 resulting in two sets of responses. This test is reproduced in figure 6.4 to display the small effect for the two different sets of node-pair capacitances in table 6.3.

6.2 Test circuit

6.2.1 Introduction

A test circuit with the circuit in [3] as a base was designed in PCBoards and manufactured by Kretselektronik AB. Surface mounted components and a SMA connector were used to minimize unwanted radiation.

Since this circuit differs from the one in [3] new PEEC model parameters were calculated i.e. the partial inductances and capacitances. No cell resistivity is used and the calculation of the capacitances does not include the dielectric substrate.

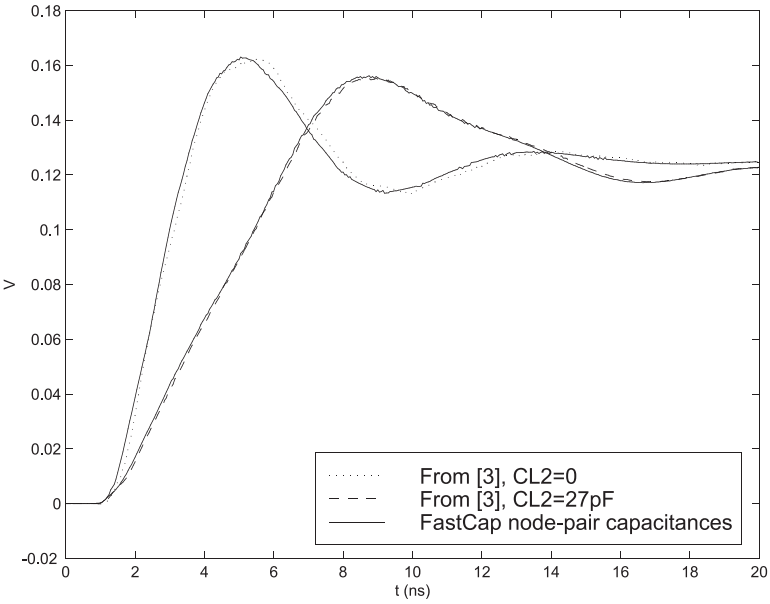

Figure 6.4: Time domain response

6.2.2 Partial inductances

When calculating the partial inductances a simplified model excluding the traces for CL_1(grey marked trace in figure 6.5) was used. With this approximation one self term and seven mutual coupling terms could be left out and the resemblance with [3] were improved.

6.2.2.1 Partial self inductances

All self partial inductances were computed by using the KS equation with the parameters in table 6.4 and the cross section 1.2mm$\times$50μm.

Self ind. term	Length. [mm]	Result. [nH]
Lp11	59.2	59.9
Lp22	2.7+3.3+4.9	1.14+1.50+2.59=5.23
Lp33	60.8	61.8
Lp44	16	12.1
Lp55	24	20.0
Lp66	60.8	61.8
Lp77	20.5	16.4

Table 6.4: Self inductances for the test circuit

Since Lp22 is subdivided by the two surface mounted resistors the contributions from the three subconductors are added to form the total self inductance.

6.2.2.2 Partial mutual inductances

All mutual partial inductances were computed by using the TT equation. Lp27 and Lp45 were also computed from their self inductances since they correspond to the special case for conductors on the same axis, chapter 3.2.3.1. For the test circuit PEEC model Lp24, Lp25 and Lp47 are used even though the coupling is weak and could be left out. Table 6.5 shows the parameters used with the TT equation for calculation of mutual partial inductances.

Mutual ind. term	Length con. 1 (mm)	Length con. 2 (mm)	Diff. x center coord. (mm)	Diff. y center coord. (mm)	Result (nH)
Lp13	59.2	60.8	2	16	15.2
Lp16	59.2	60.8	0.8	24	11.6
Lp24	13.5*	16	2.45	60.8	0.35
Lp25	13.5*	24	20	60.8	0.50
Lp27	13.5*	20.5	18.2	0	1.92
Lp36	60.8	60.8	1.2	40	8.11
Lp45	16	24	20	0	2.65
Lp47	16	20.5	18.85	60.8	0.51
Lp57	24	20.5	1.15	60.8	0.80

* Effective length for inductive partition 2, ($L_{with\ R1+R2}$+$L_{without\ R1+R2}$) / 2

Table 6.5: Mutual inductances for test circuit

To recalculate Lp27 equation 3.11 was used, for conductors on the same axis separated by a distance, with the parameters in table 6.6. All self inductances in table 6.6 and 6.7 are calculated with the KS equation.

Mutual ind. term. Lp_{km}	l_k (mm)	l_m (mm)	Separation distance l_n.(mm)	Lp_{ll} (nH)	Lp_{qq} (nH)	Lp_{oo} (nH)	Lp_{nn} (nH)	Result (nH)
Lp27	13.5	20.5	1.2	32.0	10.8	17.6	0.35	1.98

Table 6.6: Parameters for calculating Lp27

Finally Lp45 was recalculate using equation 3.10 with the parameters in table 6.7.

Mutual ind. term. Lp_{km}	l_k. (mm)	l_m. (mm)	Lp_{kk} (nH)	Lp_{mm} (nH)	Lp_{ii} (nH)	Result (nH)
Lp45	16	24	12.0	20.0	37.3	2.65

Table 6.7: Parameters for calculating Lp45

We can see that the agreement for these special cases are good. But for practical evaluation of the mutual inductances this is not a shortcut since the TT equation is well suited for computer implementation.

6.2.3 Partial capacitances

For the test circuit PEEC model the partial capacitances were used since the condition in equation 5.1 is met for frequencies approximately under 800MHz (The largest distances between two capacitïve partitions can never exceed 103mm). FastCap were used for the calculations and the geometry was programmed in the generic file interface described in chapter 4.2.2.1. The programmed geometry can be seen in figure 6.5, note that the trace for CL_1, marked grey in figure 6.5, excluded in the inductive calculations is present in a simplified format.

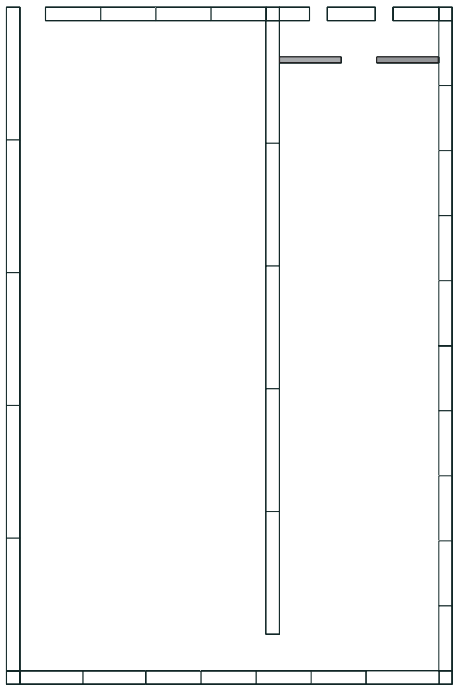

Figure 6.5: Input geometry for FastCap calculations

The resultant short circuit capacitance matrix is recalculated to the capacitance matrix

$$\mathbb{C} = \begin{bmatrix} 457 & 202 & 85 & 56 & 168 \\ 202 & 324 & 63 & 9 & 44 \\ 85 & 63 & 258 & 55 & 38 \\ 56 & 9 & 55 & 135 & 63 \\ 168 & 44 & 38 & 63 & 532 \end{bmatrix} \text{fF} \tag{6.4}$$

From this the node-pair capacitances are calculated to

$$\mathbb{C}_n = \begin{bmatrix} 0 & 289 & 154 & 92 & 310 \\ 289 & 0 & 112 & 35 & 145 \\ 154 & 112 & 0 & 75 & 118 \\ 92 & 35 & 75 & 0 & 105 \\ 310 & 145 & 118 & 105 & 0 \end{bmatrix} \text{fF} \tag{6.5}$$

If we compare these matrices with the one for the original circuit, 6.2 and 6.3, we see that the capacitances involving partition 2 has been raised. This is because of the trace for CL_1 that was absent in the original circuit.

6.2.4 (L,C)PEEC model

The resultant (L,C)PEEC model for the test circuit can be implemented in a PSpice text file as

```
PSpice_AD file for (L,C)PEEC
; External components
RL1                    8      9      300
RL2                    9      1      51
CL1                    8      1      10p
CL2                    10     4      10p
; Partial self inductances
Lp11                   10     1      59.9n
Lp22                   2      8      5.23n
Lp33                   3      2      61.8n
Lp44                   4      3      12.1n
Lp55                   5      4      20.0n
Lp66                   6      5      61.8n
Lp77                   1      7      16.4n
; Partial mutual inductances
K13                    Lp11   Lp33   0.25
K16                    Lp66   Lp11   0.19
K24                    Lp44   Lp22   0.04
K25                    Lp55   Lp22   0.05
K27                    Lp22   Lp77   0.21
K36                    Lp66   Lp33   0.13
K45                    Lp44   Lp55   0.17
K47                    Lp44   Lp77   0.17
K57                    Lp77   Lp77   0.04
```

```
; Partial self capacitances
C11                    1  0  457f
C22                    2  0  324f
C33                    3  0  258f
C44                    4  0  135f
C55                    5  0  532f
; Partial mutual capacitances
C12                    1  2  202f
C13                    1  3  84.8f
C14                    1  4  56.1f
C15                    1  5  168f
C23                    2  3  62.6f
C24                    2  4  9.25f
C25                    2  5  44.1f
C34                    3  4  54.8f
C35                    3  5  38.0f
C45                    4  5  63.3f
```

In this text file nodes 0, 8, 9, 10, are introduced to handle the external components. Node 0, not defined, will work as the reference to which all self partial capacitances are connected. All tests performed later will be based on this circuit description.

Chapter 7

Input impedance test

The input impedance of a circuit as a function of frequency is interesting when matching driving circuits and loads. To know at what frequencies to expect perfect matching and thus maximum power delivery is important in many EMC applications and antenna theory. The input impedances of the test circuit were measured with a network analyzer, and simulated with the equivalent circuit model developed in chapter 6.2

7.1 Input impedance without CL2

The input impedances were measured with a 0.1m RG223 coax cable connected between the test circuit and network analyzer.

For these simulations CL2 is not removed from the text file, it is only given a small value.

In PSpice you can model coax cables with a lossless or lossy representation [23]. For the lossless coax representation only a characteristic impedance and delay time is given. For a 0.1 m RG 223 coax cable the characteristic impedance is 50Ω. The delay time is expressed as

$$T_d = \frac{d}{c \cdot v_f} = \frac{0.1}{3 \cdot 10^8 \ \cdot \ 0.66} = 0.51ns \tag{7.1}$$

where d is the length of the coax, c is the speed of light and v_f is the velocity factor for the coax. To simulate the input impedance for the test circuit we use the equivalent circuit developed in chapter 6.2.4 completed with a AC source and proper analyze setup. This is done by adding following to the text file

```
Vin 11 0 AC 1 0 ;1 volt AC source
T1 11 0 7 6 Z0=50 Td=0.51ns ; Lossless coax cable representation
R_out 6 0 1m; Coax outer conductor DC resistance
.
.
. Text file from chapter 6.2.4
.
.
.AC lin 3000 100k 1000MEG ; Linear AC analysis from100kHz to 1GHz
.Probe
.End
```

The result from this computer simulation can be seen in figure 7.1.

The lossy representation requires all four distributed parameters, C-L-R-G, for the coax together with its length. Since C is 101 pF/m, from coax cable specifications, L can be calculated from the equation for the phase velocity (the denominator in equation 7.1)

$$v_p = \frac{1}{\sqrt{LC}} \tag{7.2}$$

resulting in 253 nH/m. The two remaining parameters, R and G, are associated with the losses in the cable and must be implemented frequency dependent. This can be done by using the damping given in the cable specifications together with a fixed G resulting in a frequency varying R. I practical situations G is usually neglected but since PSpice only accept nonzero values for the distributed parameters G is chosen to be a small value, 10μmhos. R is obtained from the equation for the attenuation constant

$$\alpha = \frac{1}{2}\left(R\sqrt{\frac{C}{L}} + G\sqrt{\frac{L}{C}}\right) \tag{7.3}$$

This has been done for some selected frequencies and the result is in table 7.1.

Frequency. (MHz)	Attenuation, α. (mNp/m)	R. (Ω/m)
500	36.8	3.66
600	40.9	4.06
700	44.4	4.42
800	48	4.78

Table 7.1: Frequency dependent R for RG 223

Since its only possible to use one R at the time for a single frequency sweep in PSpice the appropriate one for the specific application must be chosen. The input impedances were measured in the frequency range from 100kHz to 1GHz, so the R for 500MHz was used. This results in to much damping for low frequencies and to small for high frequencies.

The correct implementation for the lossy case is obtained by changing

T1 11 0 7 6 Z0=50 Td=0.51ns

as for the lossless case, to

T1 11 0 7 6 Len=0.1 C=101p L=253n G=10u R=3.66

in the PSpice text file. The result from this computer simulation together with the lossless case and the measured values can be seen in figure 7.1.

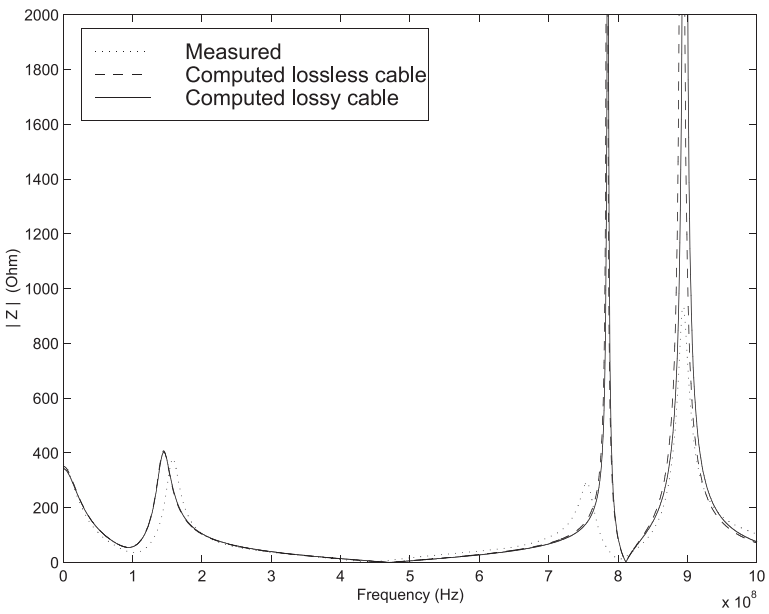

Figure 7.1: Input impedance with 0.1 m coax cable and CL2=0

The result is quite good for this (L,C)PEEC model and we see the difference for the lossy and lossless simulations are small in this application with only a 0.1m coax cable.

A computer simulation was done with the node-pair capacitances in matrix 6.5. The result is presented in figure 7.2 and the agreement is not as good as for the terminal capacitances. With this capacitance representation the PEEC model failed to accurate model all peaks in the input impedance.

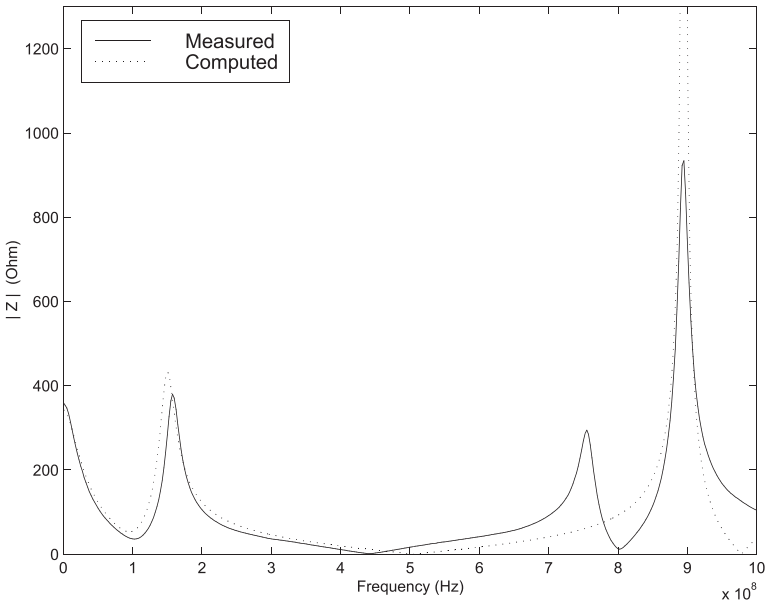

Figure 7.2: Input impedance with node-pair capacitances

7.2 Input impedance with CL2

When simulating with CL2 we use the same file as in chapter 7.1 with the correct value for CL2, which is 10pF. The simulation is done for the lossy cable according to the previous chapter and the results with the measured input impedance can be seen in figure 7.3.

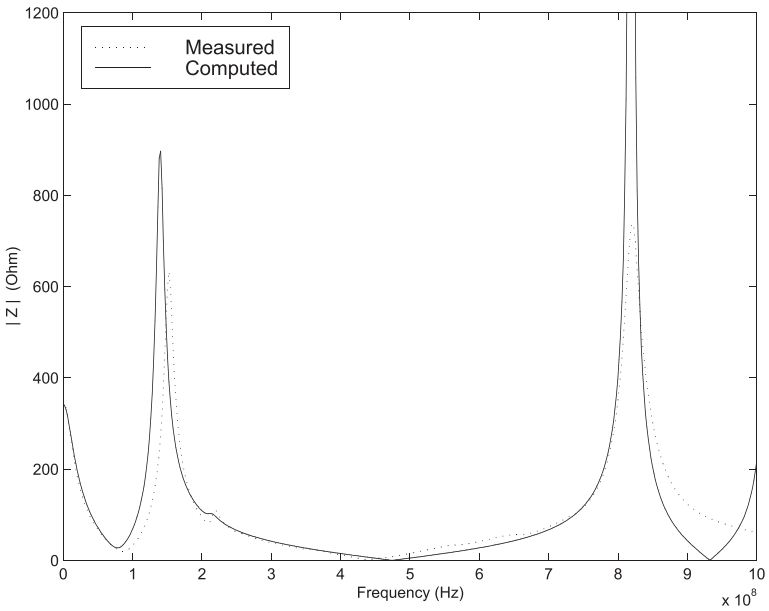

Figure 7.3: Input impedance with 0.1m coax cable and CL2=10pF

The agreement is also good in this case, even the small peak around 220MHz was found. But for the highest frequencies, > 850MHz, the PEEC model failed to predict

the input impedance. This could probably be corrected with a retarded PEEC model representation with partial coefficients of potential.

The special node-pair capacitance representation have also been tested when CL2≠0 with the same conclusions as in chapter 7.1.

7.3 Summary

As we have seen in the proceeding sections the input impedance of a circuit can successfully be computer simulated with the PEEC model.

The deviations in the simulations compared to the measured input impedances can originate from the approximate partial capacitances calculated by FastCap. To improve the results in this application, the capacitances should be calculated with the dielectric area present and the model should be completed with cell resistivity to model the losses in the traces.

To be able to simulate a frequency dependent attenuation would improve the results i.e. cut the peaks for the higher frequencies and raise the peaks for the lower. If that's not possible several small frequency intervals could be used to cover the measurement range.

Chapter 8

Radiated field test

One of the goals of this paper was to examine how accurate electric field radiation could be predicted with a PEEC model. In this test the electric far field strength for the test circuit is measured in the anechoic chamber at EMC Center, LTU. These measurements are compared with the field strengths calculated from the PEEC model currents with a simplified far field equation.

8.1 The test setup

The test circuit is put on a plastic turn table in the same horizontal plane as the receiving antenna. The circuit is connected to the signal generator by a 6.6 m long RG 223 inside the chamber followed by a 6.1 m long RG 213 outside the chamber. The bi-log antenna is connected to the test receiver with a 9.0 m long RG 213.

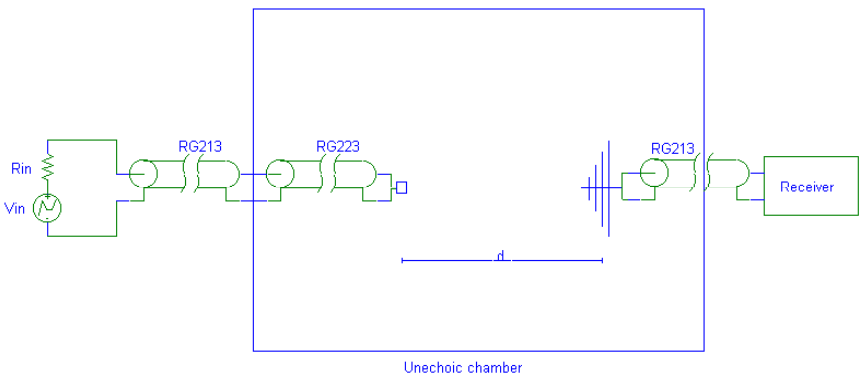

Figure 8.1: Test setup for field strength measurements

To be sure to measure the electric far field for the test circuit the minimum distance to the receiving antenna must be defined. A rule of thumb is that to be sure to measure in the far field, the distance, d, to the antenna is usually taken to be the larger of

$$d > \frac{2D^2}{\lambda} \tag{8.1}$$

or

$$d > 3\lambda \tag{8.2}$$

where D is the maximum dimension of the test circuit. The reason to why the far field was measured, is that the calculations from the PEEC model currents to theoretical field strength, performed in chapter 8.3.2, are much easier than for the near field. Since D is 206 mm, the distance to the far field region is 2.25 m for 400 MHz. This is the minimum frequency for this test and will never be used since the distance between the test circuit and receiving antenna was approximately 3 m for all tests performed. The reason is that all legislational electrical field strengths limits are defined for 3 or 10 meters. The maximum frequency is set by the PEEC model upper frequency limit, chapter 6.2.3, which is approximately 800 MHz.

8.2 Measurements

All measurements were done in the horizontal plane of the test circuit, rotating it 360° with the turn table in 10° steps. Repeated measurements for selected frequencies were done to eliminate bias and uncertainties that all EMC measurements are susceptible for. From the receiver value, antenna factor and cable losses the corresponding E-field were calculated.

8.2.1 Receiver

The receiver was a R/S EMI Test Receiver ESPC giving the average induced voltage in the bi-log antenna in dBμV.

8.2.2 Antenna factor

The antenna factor relates the received voltage to the incident electric field. It can be defined as the ratio of the incident electric field at the surface of the measurement antenna to the received voltage at the antenna terminals. The antenna factor is usually provided by the manufacturer in dB with units of inverse meters. The antenna factor for the Chase bi-log antenna used in the measurements are given in table 8.1.

Frequency (MHz)	Antenna factor (dB/m)
600	18.4
700	18.6
800	19.6

Table 8.1: Antenna factor for Chase bi-log antenna

8.2.3 Cable losses

Since the cable connecting the antenna with the receiver is long and the frequencies of interest are high the cable losses become significant. To increase accuracy, these losses need to be added to the measured value of the voltage out of the antenna to compensate for the losses. Cable losses together with the corresponding distributed cable parameter R, chapter 7.1, needed for PSpice simulations is shown in table 8.2.

	Coax cable RG 213		Coax cable RG 223	
Frequency (MHz)	Attenuation (dB/m)	R (Ω/m)	Attenuation (dB/m)	R (Ω/m)
600	0.171	1.994	0.355	4.063
700	0.186	2.116	0.386	4.420
800	0.202	2.302	0.417	4.776

Table 8.2: Cable losses used in the calculations

As we can see the cable losses are important in this case, as for the 9 m long RG 213 connecting the antenna with the receiver, the cable loss is 1.82 dB at 800 MHz.

8.2.4 Resulting electric field

The receiver voltage, antenna factor and cable losses are added together to form the resulting electric field strength as

$$E(dB\mu V/m) = V(dB\mu V) + AF(dB/m) + CL(dB) \tag{8.3}$$

The results from the measurements are shown together with the simulated electric field strengths in chapter 8.4.

8.3 PEEC simulations

The PEEC model developed in chapter 6.2 are used to find the currents in the conducting traces. The electric field strength can then be calculated with a simplified far field equation.

8.3.1 Simulation model

To correctly model the test setup the signal generator and the two coax cables must be included in the simulations. The signal generator is equivalent to a voltage source in series with a 50 Ω resistor and the cables are modeled as lossy transmission lines described in chapter 7.1. By using this in the simulation model the attenuation in the cables and the multiple reflections caused by the mismatched test circuit will be accounted for, resulting in a more accurate model.

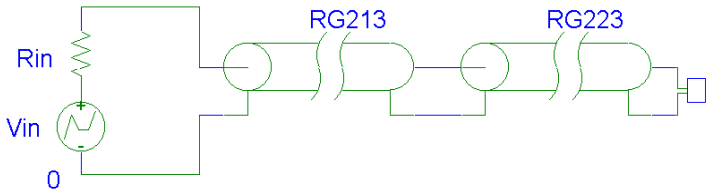

Figure 8.2: PSpice model for field strength simulation

Simulations were done for the frequencies in table 8.2 with or without CL2. The currents in the self partial inductances representing the traces were written to a text file with the print command in the PSpice text file. This ASCII file can be modified and imported in Matlab to perform the field calculations. Its important to collect the current data for a late point in time because of the reflections at the load and the signal generator. The additions to the text file, developed in chapter 6.2.4, to model the currents in the traces for the test circuit at 700MHz is shown here.

```
Vin 11 0 Sin(0 252m 700MEG 0 0 0) ; Sinusoidal excitation
Rin 11 12 50 ; Signal generator internal resistance
T1 12 0 13 14 LEN=6.1 R=2.116 C=101p L=253n G=10u ; RG 213 lossy coax
R_out1 14 0 1m ; Coax cable outer resistance
T2 13 14 7 6 LEN=6.6 R=4.420 C=101p L=253n G=10u ; RG 223 lossy coax
R_out2 6 14 1m ; Coax cable outer resistance
.
.
Text file from chapter 6.2.4
.
.
.Tran 0.075ns 405n 400n 0.0075ns ; Transient analysis fr. 400ns to 405ns
.Print tran I(Lp11) I(Lp22) I(Lp33) I(Lp44) ; Writing trace currents to file
.Print tran I(Lp55) I(Lp66) I(Lp77) I(CL1)
.Probe
.End
```

The input signal amplitude is 252mV over the signal generator internal resistance and the coax cable, that correspond to -5dBm into a 50 Ω cable. All currents are represented with 67 points, approximately 3.5 period, collected after 400ns.

8.3.2 Field calculation

When calculating the electric field from the test circuit, each trace is considered to be a short wire antenna. Under this assumption the electric far field from each trace can be

calculated using equation 8.4 developed in appendix F with help from [21].

$$\overline{E} = \frac{\mu_0}{4\pi} \frac{i \cdot \overline{l} \cdot (2\pi f) \cos(\theta)}{r} \hat{\Theta} \quad \text{(V/m)} \tag{8.4}$$

where i is the sinusoidal current in the trace, l is the trace length, θ is the angle defined in appendix F and r is the distance to the field point from the center of the trace. The equation is well suited for Matlab implementation and the result is recalculated to dBμV/m for comparison with the measured values.

8.4 Results

The electric field strengths were measured and simulated for 600, 700 and 800 MHz with the two different circuit configurations, with or without CL2. The results are viewed with the rotation angle at the x-axis and the electric field strength at the y-axis.

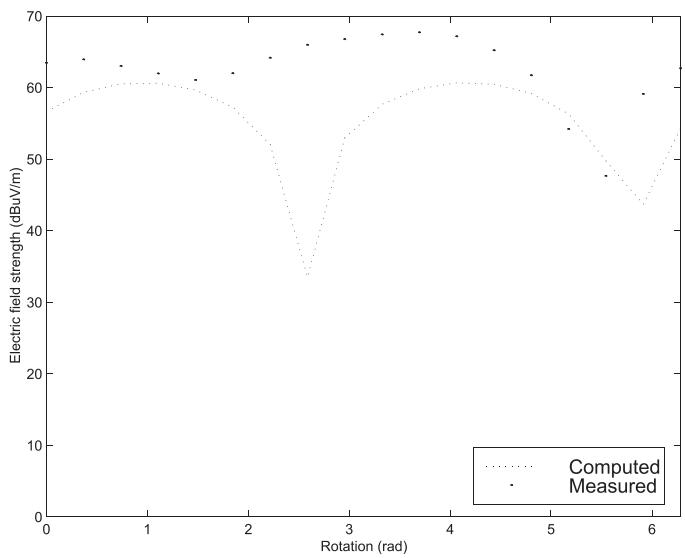

Figure 8.3: E-field for 600MHz, CL2=0

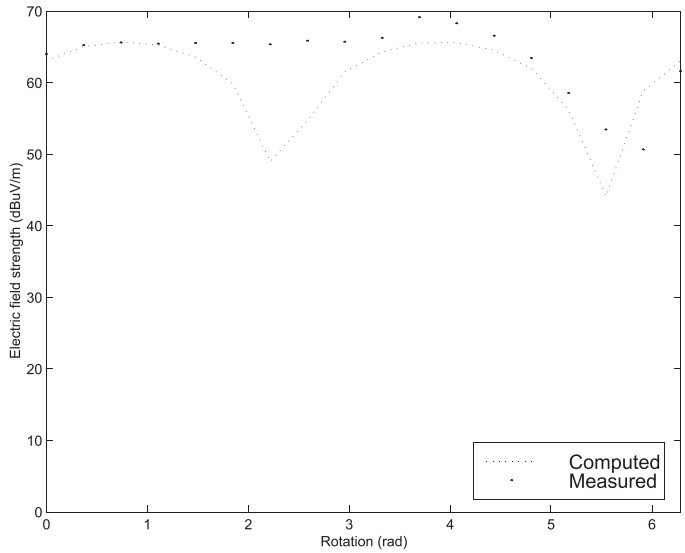

Figure 8.4: E-field for 700MHz, CL2=10pF

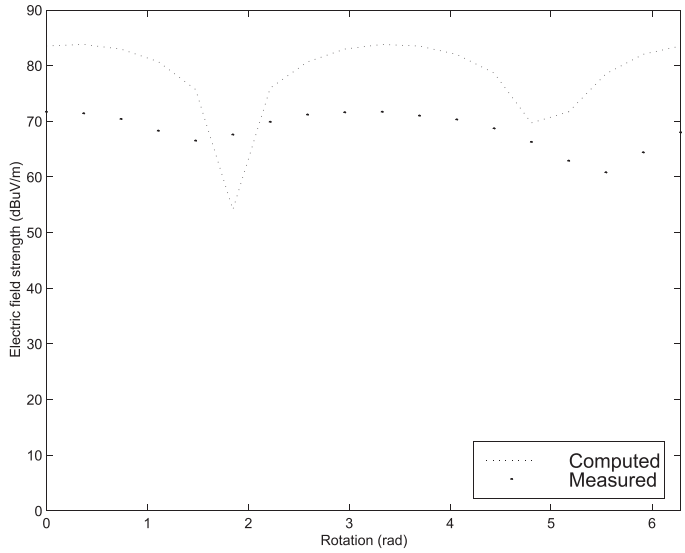

Figure 8.5: E-field for 800MHz, CL2=0

8.5 Summary

It has been shown that the PEEC model is useful when predicting the electric far field for a printed circuit board. The result is quite good for all simulations under 800MHz despite all simplifications done. This is again a reminder that the unretarded PEEC model has a upper frequency limit and this is even more important for field simulations [6].

A important notice is that the computed field strength pattern are also changing for different frequencies when some traces becomes more significant than others.

The E-field simulation test could be improved by using a retarded PEEC model and a more accurate equation for the calculations performed.

Chapter 9

Conclusions

It has been shown that the PEEC model together with PSpice is a valuable tool to predict the high frequency behavior of a printed circuit board.

Good results for the radiated electric field strength is obtained for a simplified PEEC model with rather large cells chosen.

The partial inductances should be evaluated in a computer program to improve accuracy and enable refined partitioning. This can be done in the freeware program FastHenry also supplied by MIT.

To be able to include dielectric effects in the partial capacitance calculations all PCBs should be modelled in the CAD program MSC/PATRAN. This would simplify the modeling of the geometry and increase the accuracy for the computed values.

A retarded circuit solver must be used to enable simulations of circuits with delays, thus minimize the phase errors. This is especially important when using the PEEC model for radiated field predictions and would also increase the active frequency range for the PEEC model.

Chapter 10

Further studies

The most important continuation of this paper is to use the partial coefficients of potential in a retarded circuit solver to improve the accuracy for the equivalent circuit.

Since the radiated field computations are important, a more accurate far field equation than the one used in this paper need to be developed. To verify the far field computations from the PEEC model a full wave electromagnetic solver should be used together with measurements.

Since the PEEC formulation has only been used to develope the equivalent circuit for one printed circuit board, it would be interesting to use it on a second to verify its performance.

Bibliography

[1] A. E. Ruehli, "Inductance Calculations in a Complex Integrated Circuit Environment", IBM Journal of Research and Development, vol. 16, no. 5, sep. 1972, p. 470-81.

[2] A. E. Ruehli, P. A. Brennan, "Efficient Capacitance Calculations for Three-Dimensional Multiconductor Systems", IEEE Transactions on microwave Theory and Techniques, vol. MTT 21, no. 2, feb. 1973, p. 76-82.

[3] A. E. Ruehli, "Equivalent Circuit Models for Three-Dimensional Multiconductor Systems" IEEE Transactions on microwave Theory and Techniques, vol. MTT 22, no. 3, march 1974, p. 216-21.

[4] A. E. Ruehli, P. A. Brennan, "Capacitance Models for Integrated Circuit Metallization Wires", IEEE Journal of Solid State Circuits, vol. SC 10, no. 6, dec. 1975, p. 530-6.

[5] A. E. Ruehli, P. K. Wolff, "Inductance Computations for Complex Three-Dimensional Geometries", IEEE International Symposium on Circuits and Systems, IEEE, New York, 1981, 3 vol. p. 16-19, vol. 1.

[6] A. E. Ruehli et al. "Simulating Electromagnetic Radiation of Printed Circuit Boards", 1990 IEEE International Conference on Computer-Aided Design. Nov. 11-15 1990, p. 392-395. ASBN : 0-8186-2055-2.

[7] A. E. Ruehli, H. Heeb, "Approximate Time-Domain Models of Three-Dimensional Interconnects", Proceedings, 1990 IEEE International Conference on Computer Design, VLSI in Computers and Processors, IEEE Comput. Soc. Press, Los Alamitos, CA, USA, 1990, p. 201-5.

[8] A. E. Ruehli, H. Heeb, "Retarded Models for PC Board Interconnects - or How the Speed of Light Affects your SPICE Circuit Simulation", 1991 IEEE International Conference on Computer-Aided Design. IEEE Comput. Soc. Press, Los Alamitos, CA, USA, 1991, p.70-3.

[9] A. E. Ruehli, H. Heeb, "Circuit Models for Three-Dimensional Geometries Including Dielectrics", IEEE Transactions on Microwave Theory and Techniques, vol. 40, no. 7, july 1992, p. 1507-16.

[10] A. E. Ruehli, J. Garrett, C. Paul, "Circuit Models for 3D Structures with Incident Fields", 1993 International Symposium on Electromagnetic Compatibility Symposium Record, IEEE, New York, NY, USA, aug. 1993, p. 28-32.

[11] A. E. Ruehli et al, "Stable Time Domain Solutions for EMC Problems using PEEC Circuit Models", Chicago 1994. Compatibility in the Loop. IEEE International Symposiun on EMC. IEEE, New York, NY, USA, 1994, p. 371-6.

[12] A. E. Ruehli, C. Paul, J. Garrett, "Inductance Calculations using Partial Inductances and Macromodels", Atlanta 1995. EMC - a Global Concern. IEEE 1995 International symposium on ELectromagnetic Compatibility. Symposium Record. IEEE, New York, NY, USA, 1995, p. 23-8.

[13] A. E. Ruehli, E. Chiprout, "The Importance of Retardation in PEEC Models for Electrical Interconnect and Package (EIP) Applications", Electrical Performance of Electronic Packaging. IEEE, New York, NY, USA, 1995, p. 232-4.

[14] A. E. Ruehli, U. Miekkala, H. Heeb, "Stability of Discretized Partial Element Eequivalent EFIE Circuit Models", IEEE Transactions on Antennas and Propagation, vol. 43, no. 6, june 1995, p. 553-9.

[15] A. E. Ruehli, "Partial Element Equivalent Circuit (PEEC) Method and its Application in the Frequency and Time Domain", Santa Clara 1996. EMC: Silicon to Systems. IEEE 1996 International Symposium on Electromagnetic Compatibility. IEEE, New York, NY, USA, 1996, p. 128-33.

[16] A. E. Ruehli, A. Cangellaris, W. Pinello, "Transient Electromagnetic Analysis and Model Complexity Reduction using the Partial Element Equivalent Circuit Formulation", IEEE MTT-S International Microwave Symposium Digest v 1 Jun 8-13 1997, p. 63-66. ISSN: 0149-645X.

[17] A. E. Ruehli, A. Cangellaris, W. Pinello, "Stabilization of Time Domain Solutions of EFIE based on Partial Element Equivalent Circuit Models", IEEE International Symposium 1997. IEEE, New York, NY, USA, 1997, p. 966-9 vol. 2.

[18] A. E. Ruehli, C. Paul, J. Garrett, "Stability Improvements of Integral Equation Models", IEEE Antennas and Propagation Society International Symposium 1997. IEEE, New York, NY, USA, 1997, p.1810-13 vol. 3.

[19] A. E. Ruehli, "Circuit Oriented Electromagnetic Solutions in the Time and Frequency Domain", IEICE Transactions on Communications, vol. E80-B, no. 11, nov. 1997, p. 1594-603.

[20] A. E. Ruehli, W. Pinello, A. C. Cangellaris, "Hybrid Electromagnetic Modeling of Nnoise Interactions in Packaged Electronics Based on the Partial-Element Equivalent-Circuit Formulation", IEEE Transactions on Microwave Theory and Techniques, vol. 45, no. 10, pt. 2, oct. 1997, p.1889-96.

[21] I. Tagesson, "Elektromagnetisk Fältteori II", LTH, Teoretisk elektrotteknik, 1982.

[22] C. R. Paul, "Introduction to Electromagentic Compatibilty", New York, Wiley series in microwave and optical engineering, 1992. ISBN: 047154927.

[23] MicroSim Corporation, "The Design Center - Circuit Analysis Refrence Manual", version 6.1, july 1994.

[24] Lisa Kempfer, "MSC/Patran 7.5", Computer - Aided Engineering; Cleveland; Feb 1998. ISSN 07333536.

[25] K. Nabors et al. "FastCap USER´S GUIDE", sep. 1992, URL:ftp://rle-vlsi.mit.edu/pub/fftcap/fastcap-ug.ps.Z (1999-05-01)

Appendix A

KS and TS equation

Equations for self partial inductance calculations. Normalizations used: $u = l/w$ and $\omega = t/w$, where l is the length, w is the width and t is the thickness of the conductor.

KS equation.

$$\begin{aligned}
\frac{Lp_{ii}}{l} &= \frac{2\mu}{\pi}\{\frac{\omega^2}{24u}\left[\ln(\frac{1+A_2}{\omega}) - A_5\right] + \frac{1}{24u\omega}\left[\ln(\omega + A_2) - A_6\right] \\
&+\frac{\omega^2}{60u}(A_4 - A_3) + \frac{\omega^2}{24}[\ln(\frac{u+A_3}{\omega}) - A_7] + \frac{\omega^2}{60u}(\omega - A_2) + \frac{1}{20u}(A_2 - A_4) \\
&+\frac{u}{4}A_5 - \frac{u^2}{6\omega}\tan^{-1}(\frac{\omega}{uA_4}) + \frac{u}{4\omega}A_6 - \frac{\omega}{6}\tan^{-1}(\frac{u}{\omega A_4}) + \frac{A_7}{4} \\
&-\frac{1}{6\omega}\tan^{-1}(\frac{u\omega}{A_4}) + \frac{1}{24\omega^2}\left[\ln(u + A_1) - A_7\right] + \frac{u}{20\omega^2}(A_1 - A_4) \\
&+\frac{1}{60\omega^2 u}(1 - A_2) + \frac{1}{60u\omega^2}(A_4 - A_1) + \frac{u}{20}(A_3 - A_4) \\
&+\frac{u^3}{24\omega^2}\left[\ln(\frac{1+A_1}{u}) - A_5\right] + \frac{u^3}{24\omega^2}\left[\ln(\frac{\omega + A_3}{u}) - A_6\right] \\
&+\frac{u^3}{60\omega^2}\left[(A_6 - A_1) + (u - A_3)\right]\}
\end{aligned} \tag{A.1}$$

where
$A_1 = (1 + u^2)^{\frac{1}{2}}$
$A_2 = (1 + \omega^2)^{\frac{1}{2}}$
$A_3 = (\omega^2 + u^2)^{\frac{1}{2}}$
$A_4 = (1 + \omega^2 + u^2)^{\frac{1}{2}}$
$A_5 = \ln(\frac{1+A_4}{A_3})$
$A_6 = \ln(\frac{\omega+A_4}{A_1})$
$A_7 = \ln(\frac{u+A_4}{A_2})$
TS equation.

$$\frac{Lp_{ii}}{l} = \frac{\mu}{6\pi}\{3\ln\left[U + (U^2+1)^{\frac{1}{2}}\right] + U^2 + U^{-1} \\ +3U\ln\left[U^{-1} + (U^{-2}+1)^{\frac{1}{2}}\right] - \left[U^{\frac{4}{3}} + U^{-\frac{2}{3}}\right]^{\frac{1}{2}}\} \tag{A.2}$$

Appendix B

TT equation

TT equation for mutual partial inductance calculations.

$$
\begin{aligned}
Lp_{12} &= \frac{\mu}{4\pi}\frac{1}{w_1 w_2}\sum_{i=1}^{4}\sum_{j=1}^{4}(-1)^{i+j}[\frac{b_j^2 - D_z^2}{2}a_i \ln(a_i+\rho)] \\
&+\frac{a_i^2 - D_z^2}{2}b_j \ln(b_j+\rho) - \frac{1}{6}(b_j^2 - 2D_z^2 + a_i^2)\rho - b_j D_z a_i \tan^{-1}(\frac{a_i b_j}{\rho D_z})]
\end{aligned}
\tag{B.1}
$$

where
$\rho = (a_1^2 + b_j^2 + D_z^2)^{\frac{1}{2}}$
$a_1 = D_x - \frac{l_1}{2} - \frac{l_2}{2}$
$a_2 = D_x + \frac{l_1}{2} - \frac{l_2}{2}$
$a_3 = D_x + \frac{l_1}{2} + \frac{l_2}{2}$
$a_4 = D_x - \frac{l_1}{2} + \frac{l_2}{2}$
$b_1 = D_y - \frac{w_1}{2} - \frac{w_2}{2}$
$b_2 = D_y + \frac{w_1}{2} - \frac{w_2}{2}$
$b_3 = D_y + \frac{w_1}{2} + \frac{w_2}{2}$
$b_4 = D_y - \frac{w_1}{2} + \frac{w_2}{2}$
D_x, D_y, D_z are the center to center point distances.

Appendix C

Filament inductance equation

Closed form solution for the filament inductance.

$$\frac{Lpf_{mk}}{l_m} = \frac{\mu}{4\pi}\sum_{i=1}^{4}\{(-1)^{i+1}g_i \log[g_i + (g_i^2 + r^2)^{\frac{1}{2}} - (g_i^2 + r^2)^{\frac{1}{2}}\} \tag{C.1}$$

where

$g_1 = 1 + p$
$g_2 = 1 + p - v$
$g_3 = p - v$
$g_4 = p$

The normalizations used are
$v = \frac{l_k}{l_m}$, $p = \frac{D_z}{l_m}$ and $r = [(D_x)^2 + (D_y)^2]^{\frac{1}{2}}/l_m$,
where D_x and D_y are the center to center point distances and l_m and l_k are the filament lengths.

Appendix D

Equation for coefficients of potential

Closed form solution for the coefficients of potential with notations from the figure.

$$
\begin{aligned}
ps_{ij} &= \frac{1}{4\pi\varepsilon}\frac{1}{f_a f_b s_a s_b}\sum_{k=1}^{4}\sum_{m=1}^{4}(-1)^{m+k}[\frac{b_m^2 - C^2}{2}a_k \ln(a_k+\rho) \\
&+\frac{a_k^2 - C^2}{2}b_m \ln(b_m+\rho) - \frac{1}{6}(b_m^2 - 2C + a_k^2)\rho - b_m C a \tan^{-1}\frac{a_k b_m}{\rho C}]
\end{aligned}
\tag{D.1}
$$

where
$\rho = (a_k^2 + b_m^2 + C^2)^{\frac{1}{2}}$
$a_1 = a_{ij} - \frac{f_a}{2} - \frac{s_a}{2}$
$a_2 = a_{ij} + \frac{f_a}{2} - \frac{s_a}{2}$
$a_3 = a_{ij} + \frac{f_a}{2} + \frac{s_a}{2}$
$a_4 = a_{ij} - \frac{f_a}{2} + \frac{s_a}{2}$
$b_1 = b_{ij} - \frac{f_b}{2} - \frac{s_b}{2}$
$b_2 = b_{ij} + \frac{f_b}{2} - \frac{s_b}{2}$
$b_3 = b_{ij} + \frac{f_b}{2} + \frac{s_b}{2}$
$b_4 = b_{ij} - \frac{f_b}{2} + \frac{s_b}{2}$

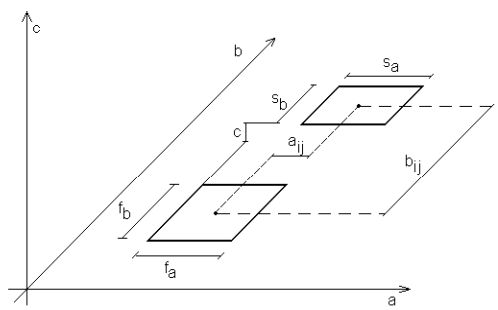

Figure for coefficients of potential calculation

Appendix E

Mail from A. E. Ruehli

Frn: ruehli@us.ibm.com <ruehli@us.ibm.com>
Till: Jonas.Ekman <jekman@sm.luth.se>
Ämne: Re: PEEC model Datum: den 22 januari 1999 15:42

.
.
.

As you know PEEC is continuing to evolve with the faster speed and higher frequencies of interest.

First to your question. The best source for the capacitance matrix transformations is given in the paper: Ruehli/Brennan "Capacitance models for integrated circuit metallization wires", IEEE Journal of solid state circuits, No.6 , Dec. 1975 pp 530-536. The capacitances in the 1974 paper may not be too accurate, since we were just at the beginning of the capacitance calculations with dielectric blocks.

.
.
.

Kind regards,
Albert Ruehli
ruehli@us.ibm.com

Appendix F

Electric field equation

To obtain the electric field from a wire antenna the definition of the vector magnetic potential, $\overline{A}(x, y, z; t)$, is used in the equation, $\overline{B} = \bigtriangledown \times \overline{A}$, describing the magnetic flux density. Resulting in the expression

$$\overline{B} = \frac{\mu_0}{4\pi} \int [\frac{j(\xi, \eta, \zeta; t - \frac{r}{c}) \times \overline{r}}{r^3} + \frac{\frac{\partial \overline{j}}{\partial t}(\xi, \eta, \zeta; t - \frac{r}{c}) \times \overline{r}}{cr^2}] dv, \tag{F.1}$$

where ξ, η, ζ are the coordinates for the volume element at the antenna, $t - \frac{r}{c}$ denotes the retardation time and r is the vector from the volume element to the field point.

When calculating the far field, $r >> \lambda$, the first term in the brackets can be left out. And by using $j = i\ d\overline{s}$ the remaining expression describing the magnetic field is

$$\overline{B} = \frac{\mu_0}{4\pi c} [\int i' d\overline{s}] \times \frac{\overline{r}}{r^2} \tag{F.2}$$

Since the physical size of the test circuit, D, is small compared to the distance to the field point, $r >> D$, all time retardations are ignored. The integral inside the brackets can be approximated with $i \cdot 2\pi f \cdot l$ resulting in the expression

$$\overline{B} = \frac{\mu_0}{4\pi c} \frac{(i \cdot 2\pi f \cdot \overline{l}) \times \overline{r}}{r^2} \tag{F.3}$$

From the notations in the figure the expression can be rewritten as

$$\overline{B} = \frac{\mu_0}{4\pi c} \frac{i \cdot (2\pi f) \cdot \overline{l} \cdot \cos(\theta)}{r} \widehat{\varphi} \tag{F.4}$$

which is the resulting equation describing the magnetic field.

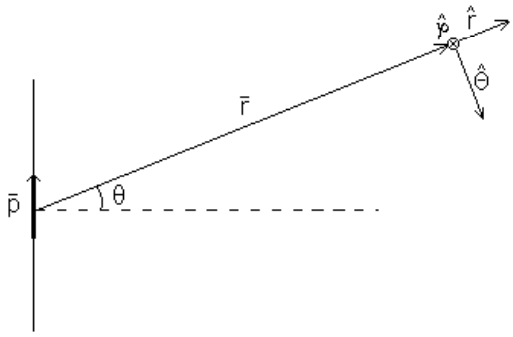

Figure for E-field calculations

From the equation describing the magnetic flux density and the electric field strength, $\overline{E} = c \cdot \overline{B}$, and the fact that $\overline{B}$, $\overline{E}$ and the vector $\overline{r}$ is forming a right hand system the electric field can be written as

$$\overline{E} = \frac{\mu_0}{4\pi} \frac{i \cdot \overline{l} \cdot (2\pi f) \cdot \cos(\theta)}{r} \widehat{\Theta} \tag{F.5}$$

This is the equation used to calculate the resulting electric field from each inductive partition in the test circuit.